ON THE PERFORMANCE OF INFRARED SENSORS IN EARTH OBSERVATIONS

by

L. F. JOHNSON

August 1972

supported by
National Aeronautics and Space Administration
NASA Grant NsG 239-62
NASA Contract NAS 9-11155

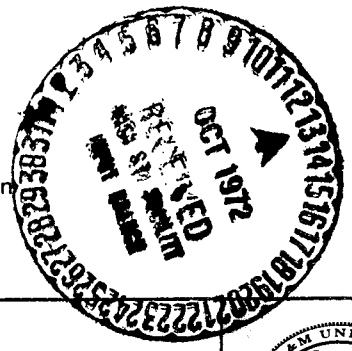

TEXAS A&M UNIVERSITY
REMOTE SENSING CENTER
COLLEGE STATION, TEXAS

Technical Report RSC-37

ON THE PERFORMANCE OF INFRARED SENSORS IN EARTH OBSERVATIONS

by

L. F. Johnson

August 1972

supported by

National Aeronautics and Space Administration

NASA Grant NsG 239-62

NASA Contract NAS 9-11155

ABSTRACT

The performance of infrared sensing systems is dependent upon the radiative properties of targets in addition to constraints imposed by system components. The unclassified state-of-the-art of infrared system performance figures is reviewed to indicate the relevance to system performance of target radiative properties. A theory of rough surface scattering is developed which allows the formulation of the reflective characteristics of extended targets. The thermal radiation emission from extended targets is formulated on the basis of internal radiation characteristics of natural materials and the transmissive scattering effects at the surface. Finally, the total radiative characteristics may be expressed as functions of material properties and incident and received directions, although the expressions are extremely complex functions and do not account for the effects of shadowing or multiple scattering. It is believed that the theory may be extended to include these effects and to incorporate the local radii of curvature of the surface.

ACKNOWLEDGEMENTS

I would like to express my sincere appreciation for the financial support of this research, provided by the National Aeronautics and Space Administration under NASA Grant NsG 239-62 and NASA Contract NAS 9-11155. The professional guidance provided by Dr. J. W. Rouse throughout the course of this research is gratefully acknowledged as it has provided a new insight into the true meaning of professionalism. The assistance in preparation of the final manuscript by Professor Jack T. Kent of the Mathematics Department and Dr. J. L. Stone of the Electrical Engineering Department, Texas A&M University, is gratefully acknowledged.

TABLE OF CONTENTS

Chapter Page

Chapter Page

LIST OF FIGURES

CHAPTER I

INTRODUCTION

The measurement or identification of some property of an object (target) without making physical contact between the target and the sensor is the essence of the remote sensing mission. Detection and measurement of any phenomenon which exhibits a dependency on the target characteristics may serve to accomplish this mission, although electromagnetic sensing is particularly suited to the remote sensing task. In fact, the predominance of electromagnetic remote sensing has become such that "remote sensing" effectively implies the detection and measurement of electromagnetic radiation.

Remote Sensing

The target characteristics which may influence electromagnetic radiation (type of material, temperature, surface state) are geophysical in nature. As a result, the primary applications for remote sensing include identification or measurement of geophysical phenomena. Secondarily, the geophysical state may be related to various other

phenomena which are not directly detectable, but the basic problems involved in geophysical interpretation remain. Various non-geophysical situations which are accompanied by remotely detectable geophysical phenomena are consequently detectable by remote sensing techniques. For example, seed germination may be detected by measurement of the associated temperature change which is known to occur during germination.

Remote sensing using airborne sensors has made possible the rapid acquisition of geoscience data over large areas without significant increase in cost over conventional methods. The shorter acquisition time associated with airborne coverage is responsible for a consequent improvement in accuracy of the data. Temporal variations are reduced to a minimum and the cost, although higher per unit time, is comparable due to the time reduction.

Successful application of remote sensing techniques has been made in numerous fields of natural and physical science: meteorology, oceanography, geology, astronomy, agriculture, ..., our environment in general, offer a multitude of potential applications. Remote sensing has been used effectively in monitoring environmental pollution, thermal mapping of the Earth's surface, ground water prospecting, detection and location of forest fires and subsurface coal fires, and early detection of diseased crops.

The primary limitation on remote sensing occurs in data interpretation. Hardware systems are capable of accurate measurements to a degree that far surpasses human or automated analysis ability. Failure to consider certain aspects of the remote sensing phenomenon and application of simplifying assumptions are responsible for questionably valid conclusions about experimental data.

An excellent introduction to remote sensing and its applications is given by D. C. Parker, et al. [1], [2], and reports of recent research are available in the Proceedings of the University of Michigan International Symposiums on Remote Sensing of Environment [3-9].

Radiation Phenomena

The remote sensing capability afforded by electromagnetic radiation may be attributed to three recognizable phenomena: emission, reflection, and propagation. Every object having nonzero absolute temperature and emissivity, emits and reflects electromagnetic energy which exhibits a dependency on various characteristics of the target. The radiation travels (propagates) away from the target in all directions and becomes incident upon the remote sensor. The frequency, phase, direction, amplitude, and polarization of the radiation indicate such target properties as temperature, type of material, and surface state

(roughness). Consequently, information about the target is conveyed to the sensor via the transmitted energy. Theoretically, the target characteristics may then be determined through proper measurement and interpretation of the resulting data, i.e. by remote sensing.

The remote sensing situation, however, is complicated by several physical phenomena. If the particular property of interest produces a measurable influence on the radiation energy, remote sensing is possible; otherwise it is not. Clearly, the influence is measurable if it is not critically deteriorated by influences from other sources. The total radiation received by the sensor is composed of radiation originating from various sources and is consequently dependent upon the characteristics of other objects in addition to the target. Radiation from non-targets may reach the sensor directly or by reflection from the target itself. The total effect of this background radiation contribution is to obscure the target radiation characteristics. Also, several characteristics of the target may affect the radiation in a similar manner such that the radiation characteristics may not be unambiguously related to the target characteristics. The total radiation, emitted and reflected from the target is also perturbed as it passes through the intervening medium to reach the sensor; scattering and absorption add further complexity to

the problem. The resulting heterogeneous combination of energy contributions and radiation phenomena does contain information, although often obscure, about the target characteristics. Interpretation of the data in view of the total radiation situation is the difficult problem of the data interpreter.

Data Interpretation

The remote sensing capability is hindered by the existing inability to interpret the resulting data accurately, frequently as a result of the interdisciplinary nature of remote sensing. Several factors contribute to the problem of interpretation, including the performance of the measuring instrument, the geophysical situation, and the particular application.

The increased use of remote sensors is accompanied by an increased misuse due to a lack of knowledge about the instrument capabilities and limitations. The ability of a remote sensing instrument to identify characteristics of an object is necessarily dependent upon the properties of the components which comprise the measuring device. Failure to consider these "sensory" constraints, some of which are common to all systems, while others vary with information requirements and system design, seriously impairs the validity of experimental results.

Much of the data interpretation problem stems from a lack of thorough understanding of the extra-sensory physical phenomena involved. The exact nature of various phenomena important in electromagnetic sensing, including natural radiation emission, scattering of electromagnetic waves from rough surfaces, and atmospheric transmission of electromagnetic radiation are not understood in detail.

The extra-sensory interpretation problem may be simplified by any of a number of assumptions about certain aspects of the total radiation situation. Any of the target, background, or intervening medium effects may be neglected or assumed to be of a certain nature at the cost of some accuracy. A common assumption is that the radiation characteristics of the target are those of a blackbody, although in nature objects may approach but do not possess blackbody characteristics. The state-of-the-art is such that these assumptions are necessary to obtain results that are valid within the restrictions imposed by the assumptions.

The interpretation problem may also be simplified for certain applications in which the reflected component of the received radiation contains the desired information. The solution is to overwhelm all of the natural radiation components with a generated radiation component having specific characteristics. After reflection from the tar-

get, the radiation may be remotely sensed as before, but interpreted more easily. Radar, for example, utilizes this approach. The complex combination of natural radiation components is suppressed as noise and the single generated component is the signal to be detected and interpreted.

Generation of this additional component is the distinguishing characteristic of an active sensing system as compared to a passive system which is designed to detect naturally occurring radiation. The utility of active and passive systems is dependent upon the particular application, or more specifically, on the particular geophysical situation to be detected. For example, active systems are useful in measurements of surface roughness or target-to-detector distance as in radar, however, passive systems prove more valuable for measuring material properties. The nature of the applicability of each type of system is revealed by comparison of their advantages and disadvantages.

The information content of the natural radiation component is high, but has been more of a hindrance than an advantage to passive sensing. Existing data interpretation techniques are unable to distinguish among the quantity of radiation contributions and phenomena which dictate the characteristics of the passive radiation component.

The active component, however, is dependent upon significantly fewer target characteristics than the passive component, and hence less information can be conveyed. The smaller quantity of information obtained by active sensing may be interpreted more easily, as the complex nature of natural radiation is suppressed as noise. The fewer variables and higher signal-to-noise ratio are responsible for a simpler data interpretation problem, although the number of applications is notably restricted by the smaller information content.

Passive sensing has not been utilized to its full capability as a result of the limited ability to interpret the resulting data. The lack of a suitable model of the total extra-sensory radiation situation is the primary limitation on interpretation ability. Combined with knowledge of sensor capabilities and limitations, such a radiation model would provide the means for more accurate and expanded applications for passive sensing.

Infrared

The electromagnetic energy spectrum consists of a continuum of frequencies from low frequency radio waves (100 Hz) to gamma rays (10^{20} Hz). It is commonly divided into bands which exhibit different characteristics, although all radiation obeys similar laws of reflection,

refraction, and propagation. The term infrared refers to that band of the spectrum which ranges from extremely high frequency radio waves (3×10^{11} Hz) to visible frequencies (3×10^{14} Hz). In terms of wavelength, the infrared band extends from 0.75μ to 1000μ. Thus infrared differs from other radiation (visible, microwave, etc.) only in wavelength and frequency.

The infrared band of the electromagnetic energy spectrum is subdivided into smaller characteristic regions, denoted near IR(NIR, 0.75μ - 3μ), middle IR(MIR, 3μ - 6μ), far IR(FIR, 6μ - 15μ), and extreme IR(XIR, 15μ - 1000μ). Each subdivision corresponds to a band of frequencies for which the Earth's atmosphere is fairly transparent (atmospheric window) or opaque as in the case of XIR.

The utility of the infrared portion of the electromagnetic spectrum has increased dramatically since the military implications became apparent during World War II. A survey of unclassified infrared literature reveals infrared systems applications in industry, medicine, and science. Indeed, any detection application is possible if a measurable variation in radiation is caused by the target property of interest. Hudson [10] has compiled a complete description of the unclassified state-of-the-art of infrared applications.

A major scientific application occurs in the area of

qualitative and quantitative remote sensing of earth resources. Passive detection and processing of infrared radiation has been applied to qualitative detection of forest fires, underground coal fires, urban development, and sea-ice reconnaissance. Quantitative applications include Gulf Stream mapping, ground water studies, air pollution and turbulence measurements, and thermal mapping of the Earth's surface. For objects having temperatures on the order of 300°K (approximate Earth temperature), a majority of natural radiation emission occurs in the infrared region of the spectrum; 30% falls in the 8-14 micron atmospheric window. Thus passive infrared detection is particularly suited to accomplishment of the remote sensing mission.

Unclassified infrared literature, however, consists primarily of qualitative investigations, and quantitative studies in which the data is frequently considered to be absolute truth with no attempt to evaluate the actual quality of the measurements. Scanner type data is often viewed as photography, without consideration of emissivity or atmospheric effects. This type of data analysis is of marginal utility and often of questionable validity.

A typical investigation has been reported by Wermund [11] in which passive microwave and infrared sensors were applied to remote sensing of ground water concentrations

in arid terrain. Two different conditions, which were considered to be indicative of "a high probability of ground water", were dense vegetation and surface moisture. Data interpretation, thus consisted of a qualitative search for anomalies in the data. Dark areas on infrared imagery were interpreted as cold due to the evaporation of surface moisture, while areas of low brightness temperature in the microwave data were interpreted as areas of low emissivity, as a result of the surface moisture.

In both cases, the results were oblivious of certain aspects of the remote sensing problem. Anomalous areas as indicated in the data were not necessarily a result of ground water, although for the particular situation (arid terrain) other geophysical effects were not likely to be responsible for the anomalous behavior. Consideration was not given to atmospheric effects, background radiation variations, or emissivity variations with no apparent data deterioration. The consistent nature of the arid terrain is responsible for minimization of these various geophysical effects and the results of the study show a high degree of accuracy in prospecting for ground water. The success may be attributed to the relative absence of deteriorating influences in the arid terrain and to the relative ease of detection of the anomalous character of ground water indicators.

Foster [12] has conducted a study of thermal mixing in effluent waters using passive infrared imagery in the 8-14μ range. The results showed an amazing accuracy in quantitative remote measurement of water temperature, although no attempt was made to account for any geophysical variables. Sensor characteristics were also neglected. Implementation of three data reduction techniques resulted in average accuracies of one to five percent.

This study has proven the capability to make gross temperature measurements under controlled conditions. The bulk of the infrared imagery pictured the effluent canals of a power generating station. The cross-sectional area and flow rate of each canal was essentially constant and surface characteristics were invariant except in the area of two cataracts. The simplified nature of the controlled experiment is responsible for the accuracy obtained. Detailed analysis of sensory and extra-sensory variables would be required for accurate and general applications.

Scope of Report

In the following chapters, the total quality of remote sensing measurements is considered. The passive infrared sensing system is of primary interest; however, the results have a degree of impact on active systems, in addition to passive sensors of other regions of the electromagnetic

spectrum.

The state-of-the-art of infrared systems and their performance is introduced in Chapter II. The infrared system is introduced schematically and the various components are evaluated in terms of their performance figures. The total instrument is then considered as a single unit with an associated performance figure.

Chapter III begins the study of extra-sensoring variables and their relation to total system performance. The topic of interest is the reflective scattering of electromagnetic radiation from target surfaces. General equations are formulated which are extremely complex and difficult to use.

In Chapter IV, generation and emission of thermal radiation is considered. The nature of internal radiation is formulated and the scattering theory of Chapter III is paralleled to describe the transmissive scattering of internal radiation to the surroundings. The resulting expressions are again very complex.

Conclusions about the theory and its limitations are included in the final chapter (Chapter V). In addition, recommendations are made for further investigation into the extension and simplification of the results which have been shown to conform to known results for the special case of a smooth surface.

CHAPTER II

INFRARED SYSTEM PERFORMANCE

The performance of an infrared sensing system is necessarily dependent upon the characteristics of the components which comprise the total system. Few publications in the open literature have addressed the total instrument performance problem, due to security classification of the subject matter. In this chapter, the performance of each component of the system will be considered individually, followed by a discussion of the total instrument system performance. A schematic representation of the basic elements of the modern infrared sensing system: optics, detector, cryogenic cooling (for certain types of detectors), electronic signal processor, and display is shown in Figure II-1 and provides a convenient arrangement for the sections that are to follow.

Optics

The purpose of infrared optical systems is to form images of real objects, which may be emitting their own radiation, reflecting radiation from other sources, or both. Any distortion in the image or loss or gain of radiant power introduced by the optical system represents imperfect performance and should be indicated in a perform-

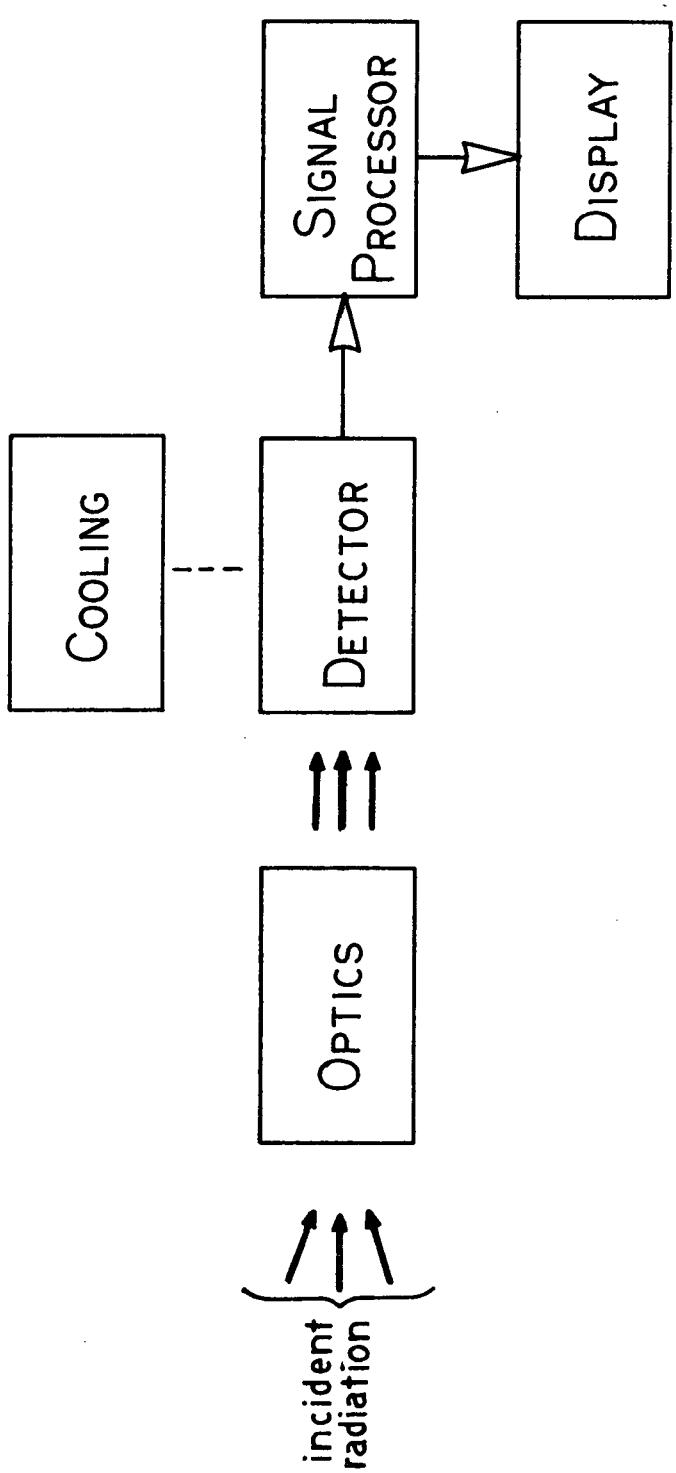

Figure II-1

Infrared Sensing System

ance figure.

Factors Affecting Image Clarity

Two processes contribute to distortion of an optical image: diffraction, due to the wave nature of radiant energy, and aberrations, caused by the optical materials. Aberrations may be controlled by the optical designer, but diffraction establishes the ultimate limit in optical performance. Diffraction limited optical systems are currently available.

Diffraction. Diffraction in optical systems occurs at the edges of optical elements and at the aperture which limits the collected radiation. Even in the absence of aberrations, diffraction still causes a point source to be imaged as a bright central disk surrounded by several alternately light and dark rings. Eighty-four percent of the radiant power is contained in the central disk called the Airy disk. The angular diameter, δ, of the Airy disk is a function of the wavelength of the incoming radiation and of the diameter of the collecting aperture, and may serve as a partial indicator of the performance of an optical system. The relationship is

$$\delta = \frac{0.244\ \lambda}{D_o} \qquad (II\text{-}1)$$

where: δ = angular diameter of the Airy disk in milliradians

λ = wavelength in microns

D_0 = diameter of the collecting aperture in centimeters

Aberrations. In optical systems, seven types of aberrations can exist, which may be categorized as either chromatic or monochromatic. Chromatic aberrations, caused by spectral variation of the indices of refraction of the lens materials, are of two types: (1) longitudinal, indicating a variation in the position of the focal point as a function of wavelength, and (2) lateral, indicating a variation in the size of the image as a function of wavelength. Although careful design of refractive optics can minimize chromatic aberrations, they are completely eliminated by the use of reflective optics.

Monochromatic aberrations, however, may occur in both reflective and refractive optical systems and include five distinct types: (1) Spherical Aberration, in which rays passing through the optics at various distances from the optical axis are not brought to a common focus; (2) Coma, in which objects located away from the optical axis image as an enlarged assymetrical comet shaped blur; (3) Astigmatism, indicated by a point located away from the optical axis being imaged as a pair of orthogonal lines; (4) Curvature of Field, in which the image of a plane object lies on

a curved rather than on a plane surface; (5) Distortion, in which straight lines not passing through the center of the field are imaged as curves.

Until recently, typical infrared optical systems have employed reflective optics predominantly, since relatively few optical materials were transparent to infrared frequencies. Lenses made of ordinary glass which are used in the visible range are useful only in the very near infrared, which has provided the impetus for research into the infrared transmission of other materials. At present, a suitable selection of infrared transmitting materials is available to provide a sufficient variety of refractive indices and dispersions (variations of refractive index with wavelength) so that achromatized compound lenses can be constructed. However, all such lens systems have only a fairly narrow operating wavelength range. For wide-band operation, extending into the middle and far infrared, lens systems must be replaced with reflective optics, which have focusing properties completely independent of wavelength, or perfectly achromatic.

Although all concave mirrors produce distorted images when the target rays arrive from directions deviating considerably from the optical axis, infrared optical systems generally cover only a small instantaneous field of view. Also, the detector is normally located near the optical

axis. As a result, only certain aberrations are of importance to most infrared systems, including spherical aberration, coma, and chromatic aberrations (if lenses are employed). Aspheric reflective surfaces can completely eliminate spherical aberration, although several thin lenses also can be combined to reduce it below the diffraction limit. The chromatic aberrations may be eliminated by the use of reflective optics so that coma is the only distortion evident for small field angles and its effect decreases with the magnitude of the field angle.

Factors Affecting Image Brightness

Radiative power lost or gained in optical processing reduces the performance of infrared systems. Diffraction can cause a part of the collected radiative power to be redirected and subsequently lost. A measure of the diffraction effect is provided by the diameter of the diffraction limited Airy disk, since 84% of incoming radiative power is contained within the disk. The linear diameter of the disk is related to the angular diameter (II-1) by the equivalent focal length of the optics

$$d = \delta f \qquad \text{(II-2)}$$

where: d = linear diameter of the Airy disk in microns

f = equivalent focal length of the optics in centimeters

δ = angular diameter of the Airy disk in milliradians given by (II-1)

If the detector is large enough to receive the entire disk but small enough to exclude the first diffraction ring, 16% of the radiation is lost due to diffraction.

The reflection, refraction, and absorption properties of the optical materials can also affect the performance of an optical system. For refractive optical elements, reflection and absorption represent energy lost; for reflective elements, transmission claims a finite amount of radiative power. The spectral transmission of the most useful infrared refractive optical materials is shown in Figures (II-2). In general, the transmittance shows a distinct spectral variation and does not exceed 90% at any wavelength for a 2 mm sample. For the far infrared region the transmittance does not exceed 70% for any of the materials; at least 30% is lost by reflection and absorption.

Reflective optical elements are inherently more efficient than refractive elements but performance is also inhibited to some degree by imperfect reflection. The reflectance of aluminum, the most common reflective optical material, exceeds 90% for wavelengths longer than 0.5

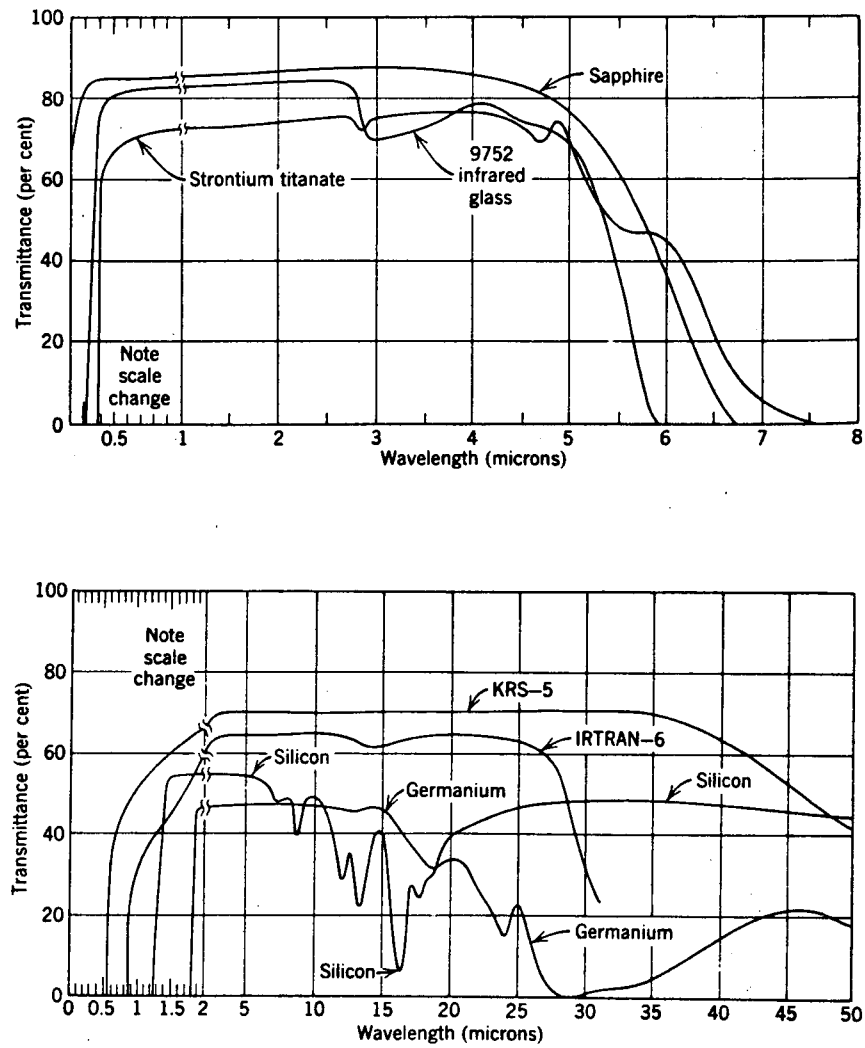

Figure II-2

Transmittances of Optical Materials [13]

micron and 98% for wavelengths longer than 8 microns, another reason for the widespread use of reflective optics in infrared systems.

The reflection from refractive optical elements may be theoretically eliminated for a single wavelength by covering the surface of the element with an antireflective coating of a specific thickness and refractive index. Although the exact thickness and refractive index are impossible to obtain, a 10% deviation in the optimum refractive index results in a decrease of only 1% in the efficiency of the coating. The reduction over a band of wavelengths, such as an atmospheric window, can be significant.

The emission of radiation by the optical elements also deteriorates the quality of the measurement since extra non-target raidation is introduced in this manner. The emittance of common optical materials is highly classified but a reasonable estimate (within 20%) may be obtained from Kirchhoff's Law, equating emittance to absorptance.

Optical modulators, called reticles or choppers, are sometimes included to provide directional information for tracking or to suppress unwanted signals from backgrounds. Reticles consist of a pattern of alternately clear and opaque areas mounted on a suitably transparent substrate and can increase the detectability of a target in the

presence of extraneous background detail. The chopping frequency is of significant importance to the overall performance of the system as is indicated in subsequent sections of this chapter.

Modern reflective optical systems for the infrared have evolved from the classical reflective systems developed for astronomy. Although in a majority of these systems the aperture is partially blocked by a secondary mirror, the angular resolution is apparently increased since a central obstruction reduces the size of the Airy disk. Unfortunately the consequence is a decreased flux in the central disk. Popular systems for infrared applications include the classical Cassegrainian, Dall-Kirkam, and catadioptric systems which employ thin correcting lenses (Schmidt, Maksutov, and Mangin Mirror). A discussion of modern optical systems for the infrared may be found in [14].

For infrared radiometers and scanners, the fundamental purpose is to measure a quantity of radiation incident from the target. Therefore the primary optical performance factor concerns the percentage of incident target radiation which arrives at the detector and the percentage of radiation arriving at the detector which did not originate at the target (factors affecting image brightness). Using the various spectral reflectances, transmittances, and

emittances of the optical elements, it is possible to arrive at an accurate estimate of the radiative power lost and gained.

Detectors

The word "detector" has a variety of connotations, but may be best described as a transducer of radiant energy. In accordance with this definition, there are precisely two types of detectors: (1) imaging, which simultaneously, form a total image of the target (examples are: photographic film or the human eye), and (2) elemental, which respond to the average irradiance from a small field of view (an effective point on the target). It is possible to build an image of a target with elemental detectors by sequentially scanning the scene or assembling a number of elemental detectors into an array thus forming an imaging detector.

It is often more convenient to group detectors into two classes that distinguish among the physical mechanisms involved in the detection process. *Thermal detectors* operate on the principle that the heating effect of incident radiation alters the electrical properties of the detector. Response is proportional to the energy absorbed. The interaction of incident photons with the electrons in a detector forms the basis for the operation of *photon* or

quantum detectors, for which, the response is proportional to the number of photons absorbed. Consequently, a plot of the theoretical response of photon detectors as a function of wavelength for a constant flux is a linearly increasing function, while thermal detector response is constant (Figure II-3).

Performance Criteria

Past research concerning infrared system quality has been largely confined to evaluation of the quality of the detector. Several performance figures have been introduced which describe the partial performance of radiation detectors, but a single number representing the total performing ability does not exist.

The detector output per unit input is of primary importance in calculations of the overall gain function of the system. The *responsivity* of a detector which is analagous to its gain is given by

$$\mathcal{R} = \frac{V_s}{H A_d} \qquad (II-3)$$

where: V_s = r.m.s. output voltage of the detector at the fundamental chopping frequency

H = irradiance on the detector

A_d = detector area

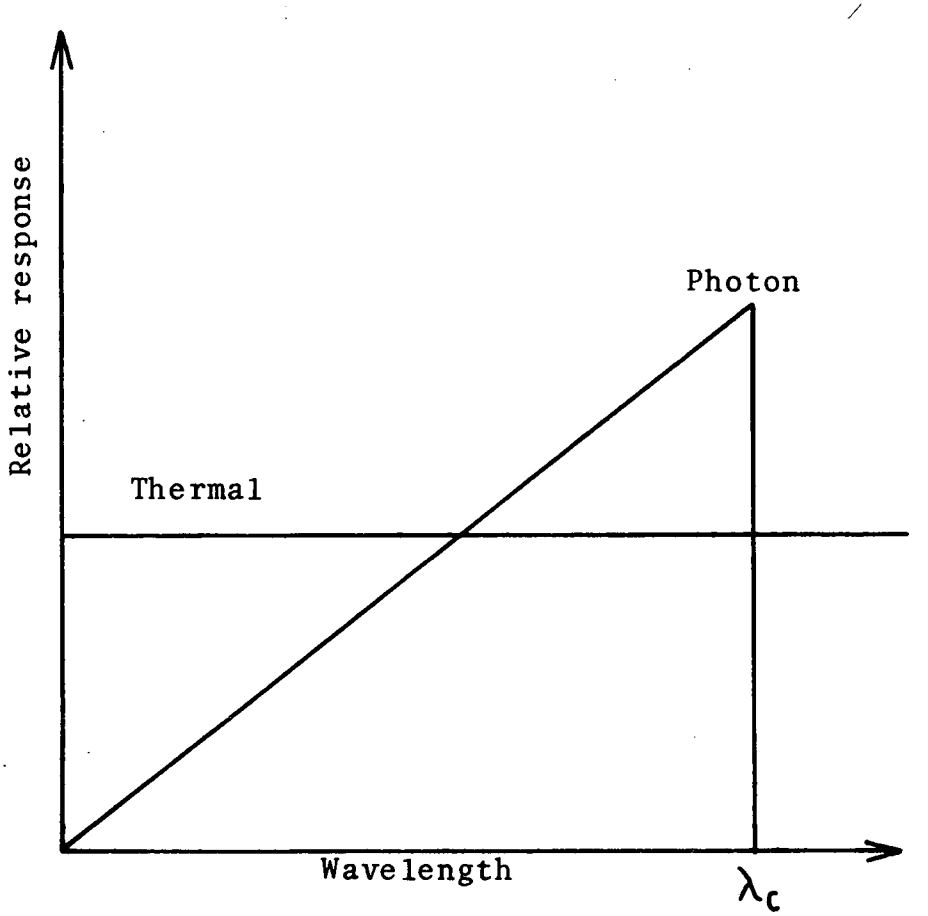

Figure II-3

Detector Spectral Response

The response time of a detector is represented by its *responsive time constant* which is defined as the time required for the detector output to reach 63% of its final value after an instantaneous change in irradiance. Many detectors respond exponentially, in which case the time constant and responsivity are related by

$$\mathcal{R}_f = \frac{\mathcal{R}_o}{(1 + 4\pi^2 f^2 \tau^2)^{1/2}} \qquad (\square\text{-}4)$$

where: $\mathcal{R}_f$ = responsivity at the chopping frequency f

$\mathcal{R}_0$ = responsivity at zero (very low) chopping frequency

τ = responsive time constant of the detector

Although responsivity is useful for gain considerations, it gives no indication of the minimum detectable radiant flux. A measure of minimum detecting ability is provided by the *noise equivalent power* (NEP). It is defined as the incident radiant power necessary to produce an output signal for which the signal-to-noise ratio (SNR) is unity, and is given by

$$NEP = \frac{H A_d V_n}{V_s} = \frac{V_n}{\mathcal{R}} \qquad (\square\text{-}5)$$

where: V_n = r.m.s. value of the noise voltage at the output of the detector

Any actual measurement of NEP must include the electrical bandwidth of the noise measurement circuit since the quantity of noise measured is dependent upon that parameter.

A similar quantity is the *noise equivalent irradiance* (NEI), given by

$$NEI = \frac{H V_n}{V_s} = \frac{NEP}{A_d} \qquad (II-6)$$

which expresses the irradiance required for a SNR of unity. The NEI concept is sometimes used as a measure of the total system quality.

Frequently, for convenience, the reciprocal of NEP, known as *detectivity* (D), is used as a performance figure. The detectivity provides a measure of performance which increases (rather than decreases) with the quality of the detector, a desirable characteristic in many performance factors.

Detectivity is a function of several variable parameters: incident radiation wavelength, detector temperature, chopping frequency, detector bias current, detector area, and bandwidth of the circuit used to measure the detector noise. There is no apparent theoretical relation-

ship between detectivity and wavelength or temperature, so the variation with these parameters must be found experimentally. It is customary to make spectral measurements at any of several easily achievable and readily reproducible temperatures such as those of approximate earth temperature (300°K), solid carbon dioxide (195°K), liquid nitrogen (77°K), and liquid helium (4.2°K). The effect of chopping frequency is negligible at low frequencies, ($f << 1/2\pi\tau$) and in many cases varies exponentially as indicated in (II-4). The detectivity has a single valued maximum with respect to bias current and is normally expressed for that value of current. Extensive theoretical and experimental studies have shown that it is reasonable to assume that detectivity varies inversely as the square root of the detector area, or

$$D A_d^{1/2} = \text{constant} \qquad \text{(II-7)}$$

provided the length of the detector sensitive area does not exceed five times the width. On the assumption that noise voltage per cycle of bandwidth is independent of frequency, detectivity varies inversely with the square root of the electrical bandwidth Δf.

An attempt to eliminate two of these variables in a

performance figure has been made by Jones [15] who introduced the quantity D*: the detectivity referred to an electrical bandwidth of 1 Hz and a detector area of 1 cm^2.

$$D^* = D(A_d \Delta f)^{1/2} \qquad (II-8)$$

This expression is valid under the assumptions of the inverse variation of detectivity with the square root of the electrical bandwidth, Δf, and the detector area, A_d. "Dee-star" as it is called, provides a convenient comparison for detectors with different areas used in circuits having different electrical bandwidths. The dimensions of D* are occasionally referred to as a "jones". The dee-star for a specific detector is expressed as D* followed in parenthesis by the temperature, chopping frequency, and/or wavelength at which the measurements were made. A comparison of D* for many common detectors is shown in Figure II-4.

If the performance of a detector is ultimately limited by background noise, it is said to be background limited. Under these conditions D* is a function of the angular field of view of the optical system, and another detectivity may be introduced which is referred to as an angular field of view of π steradians. Dee-double-star, D**, is

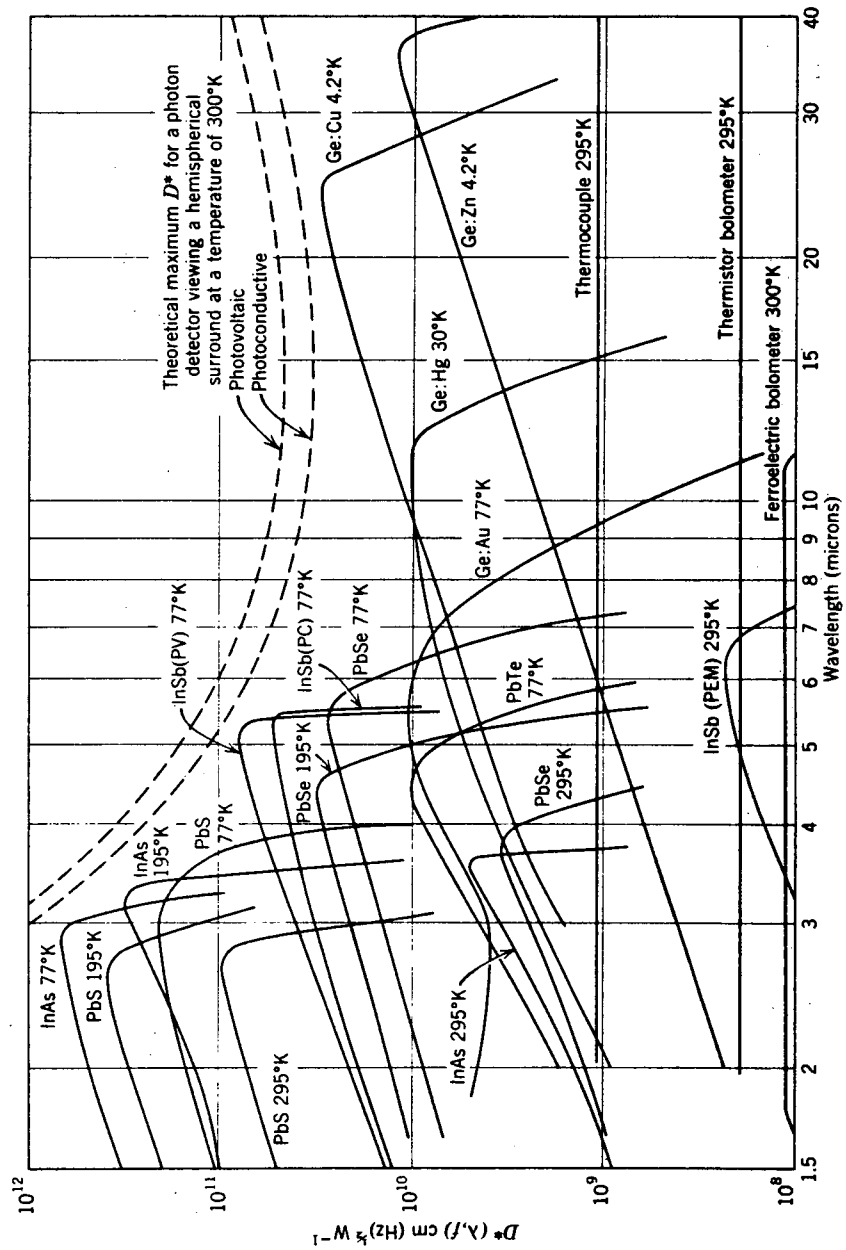

Figure II-4

Comparison of D* for Common Detectors [16]

defined

$$D^{**} = \left(\frac{\Omega}{\pi}\right)^{1/2} D^{*} \qquad \text{(II-9)}$$

where: Ω = effective field of view

Thermal Detectors

Infrared thermal detectors, most of which do not require cooling, operate by virtue of the heating effect of incident radiation on the detector characteristics. Theoretically, thermal detectors respond equally to all wavelengths, making them ideal for use in radiometers, although typical responsive time constants range from a few milliseconds to several seconds.

The first useful infrared thermal detector, the thermocouple, was not developed until about thirty years following Herschel's experiment. The voltage developed at its terminals is proportional to its increase in temperature. Typically, the electrical resistance is low (1 to 10Ω); thus, it is well suited for use with transistor amplifiers. It is, however, very fragile, generally limiting it to use in the laboratory, and its relatively long time constant restricts the allowable chopping frequency to less than 10 Hz. An approximate relationship

for the time constant has been formulated by Sanderson and stated in [17],

$$\tau = \frac{C}{\Lambda} \qquad \text{(II-10)}$$

where: C = thermal capacity of the thermoelectric junction and receiver assembly

Λ = energy loss rate of the assembly

Similarly the responsivity is approximately

$$\mathcal{R} \cong \frac{\tau}{C} \qquad \text{(II-11)}$$

Several thermocouples may be connected in series to form a thermopile, which displays increased responsivity, since the voltages are additive. Increased detector resistance simplifies impedance matching to an amplifier, but the responsive time constant, usually approaching several seconds in length, eliminates the possibility of using a chopper.

A detector which changes electrical resistance when heated by radiation is called a bolometer. Thermistor bolometers, generally rugged and uncooled, provide good field service, displaying high electrical resistance and

relatively short time constant (1 to 50 msec). Other types of bolometers include *superconducting* (operating in the superconducting regions of certain metals and semiconductors), *carbon* (with D* approximately 10 times that of a thermistor), and *germanium* (with D* approximately 100 times that of a thermistor).

An optimistic engineering estimate of the minimum obtainable NEP with thermocouples or bolometers is provided by "Haven's limit". The minimum detectable energy by a detector with area of 1 cm^2 is

$$E = 3 \times 10^{-11} \quad \text{joule}$$

which corresponds to

$$NEP = \frac{3 \times 10^{-11}}{\tau}$$

and the maximum D* obtainable is

$$D^*_{max} = 1.67 \times 10^{10} \tau^{1/2} \qquad \text{(II-12)}$$

The pneumatic or Golay detector operates on the principle that the pressure of an ideal gas increases proportionally with temperature increase due to heating by incident radiation.

The constructional materials for thermal detectors are not in themselves good absorbers and hence must be blackened by applying an absorbant coating. Ideally the coating has a uniformly high absorptance at all wavelengths, negligible thermal capacity, high thermal conductivity, and no adverse effect on the electrical properties of the detector.

Quantum Detectors

The interaction of photons with the electrons in certain materials, known as the "photo effect", forms the basis for a certain class of detectors. These photon or quantum detectors, differ from thermal detectors in that they respond to the number of incident photons rather than the quantity of incident energy, and hence their spectral response is inherently wavelength dependent. Most quantum detectors must be cooled to cryogenic temperatures. Their performance is generally very good with detectivities one or two orders of magnitude greater than typical values for thermal detectors, and very short responsive time constants (usually only a few microseconds).

Intrinsic photon detectors are long wavelength limited to less than 7 μ since all currently available intrinsic materials have forbidden energy gaps in excess of 0.18 at room temperature, although a slight increase in cutoff wavelength can be obtained by cooling. It is also possible to control the value of the cutoff wavelength by doping an alloy of silicon and germanium. A photoconductive detector has been produced in this manner and is useful in the 8-14 micron range, although a minimum of cooling is required.

The "photo effect" can be classified into two types; external, typified by electrons escaping the surface of the material, and internal, involving the generation of charge carriers within the material. The external type is rarely used in the infrared since it has a long wavelength limit dictated by the work function of the surface. Photon detectors based on internal photo effect include photoconductive, photovoltaic, and photoelectromagnetic type detectors.

Photoconductive detectors generate electron-hole pairs when illuminated by incident photons, resulting in a variation in conductivity. The varying conductivity modulates the current in a load resistor which is normally connected in series with the detector and a dc power supply. Any noise in the power supply will deteriorate the resulting signal. The responsivity of an extrinsic

photoconductive detector of 1 cm^2 area is given by

$$\mathcal{R} = \frac{\eta t_c \mu e}{x \sigma} \qquad (II-13)$$

where: η = quantum efficiency (number of charge carriers produced per incident photon)

t_c = average carrier lifetime

μ = mobility of the carriers

e = electronic charge

x = detector thickness

σ = detector conductivity

The maximum theoretical D* for the blip (background limited photodetector) condition is

$$D^* = 2.52 \times 10^{18} \lambda \left(\frac{\eta}{Q_b}\right)^{1/2} \qquad (II-14)$$

where Q_b is the background flux. This theoretical limit is included in Figure II-4, p. 31, to show the degree to which modern detectors attain theoretical perfection.

To insure proper utilization of the entire volume of the detector, fairly transparent materials are used with reflective coatings on the side opposite the illumination direction. Intrinsic materials such as silicon, germanium,

lead sulfide, lead selenide, indium arsenide, and indium antimonide are well suited for photoconductive detection as well as germanium doped with gold, cadmium, mercury, copper, or zinc.

A self generating detector (not requiring bias) may be constructed by forming a p-n junction in an appropriate semiconductor material. Incident photons generate electron-hole pairs which are subsequently separated by the electric field at the junction, increasing the voltage across the junction, hence the term *photovoltaic* detector. The theoretical maximum detectivity is 40 percent greater than for phtoconductive detectors, and is given by

$$D^* = 3.56 \times 10^{18} \lambda \left(\frac{\eta}{Q_b}\right)^{1/2} \qquad \text{(II-15)}$$

which is also shown in Figure II-4, p.31, although response is again limited to 7 μ. Common photovoltaic detectors are constructed of silicon, indium arsenide, or indium antimonide and are occasionally referred to as "photodiodes".

Electron-hole pairs generated by incident photons in an intrinsic semiconductor material may be separated by an externally applied magnetic field. Detectors of this type are called *photoelectromagnetic* and provide very short responsive time constants, although the detectivity is

lower than that of typical photoconductive or photovoltaic detectors. Response to 7 μ can be obtained without cooling.

If the performance of a detector is ultimately limited by its own internal noise, an increased D* can be obtained by placing it in optical contact with a lens. The SNR and D* are increased by a factor n_s, the refractive index of the lens.

Noise

Spurious fluctuations (noise) in the detector output signal, a result of a stochastic or random process, impose limitations on the performance of infrared systems. Several types of noise are of importance in infrared systems, including Johnson noise, generation-recombination noise, radiation or photon noise, temperature noise, and several types which vary inversely with frequency, termed 1/f noise. Two of these, Johnson and 1/f noise, occur in both thermal and quantum detectors, while temperature noise occurs only in thermal detectors and generation-recombination and photon noise occur only in quantum detectors.

Johnson, or thermal noise, occurs in all conducting materials: a consequence of the random electron motion. The mean square noise voltage, or current per unit band-

width, is independent of frequency, a characteristic prompting the term "white" noise, and is given by

$$\overline{V^2} = 4kTR\Delta f \qquad \text{(II-16)}$$

where: k = Boltzmann's constant

T = detector temperature

R = detector resistance

Δf = electrical bandwidth of the circuit

Johnson noise is the predominant noise source in detectors at very high frequencies. At slightly lower frequencies, 1/f noise is apparent. The power spectrum in this region is generally expressed,

$$P(f) = \frac{c\,(I_{dc})^{\alpha}}{f^{\beta}} \qquad \text{(II-17)}$$

where: c = proportionality constant

I_{dc} = dc bias current

The symbols, α and β are characteristics of the particular detector. Generation-recombination noise is restricted to photon detectors and is a result of the random nature of electron-hole generation and recombination. It is the

major source of noise at intermediate frequencies below which 1/f noise again prevails.

The bandwidth of a noise signal is difficult to define if it does not display "white" characteristics. To alleviate this problem, an equivalent noise bandwidth is defined by

$$\Delta f = \frac{1}{g(f_o)} \int_o^\infty g(f)\,df \qquad \text{(II-18)}$$

where: $g(f_o)$ = peak value of the noise power gain

$g(f)$ = power gain at frequency f (Figure II-5)

Statistically, noise is described by a normal (Gaussian) probability density function

$$P(x) = \frac{1}{\sigma(2\pi)^{1/2}} \exp\frac{-(x-\bar{x})}{2\sigma^2} \qquad \text{(II-19)}$$

where: $\bar{x}$ = mean noise level (voltage or current)

σ = standard deviation from the mean

The noise contributed by a single system component is represented by its noise factor, F, which is the ratio of the SNR at its input to the SNR at its output. It is sometimes convenient to express the noise factor in

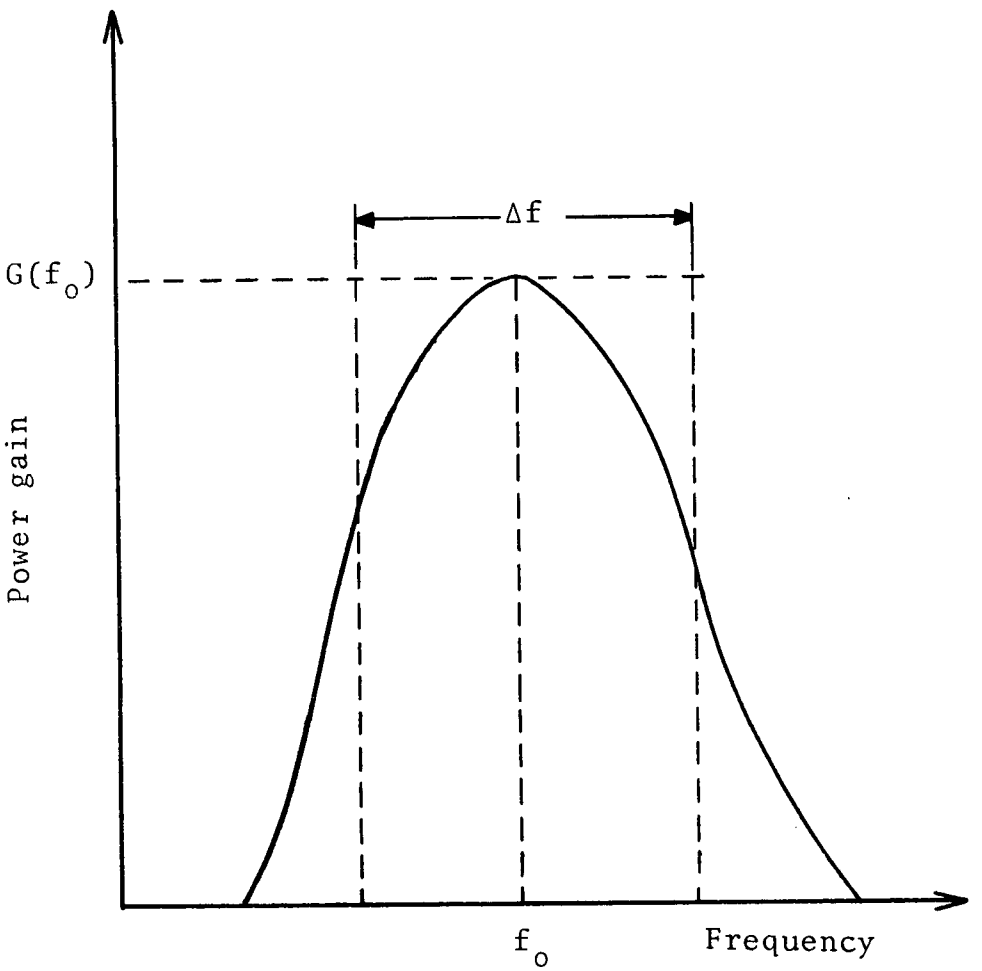

Figure II-5

Equivalent Noise Bandwidth

decibels, in which case the correct term is "noise figure".

No satisfactory data have appeared on the range over which the response of a detector is linearly proportional to irradiance, although most photon detectors respond linearly over a range extending to 4 orders of magnitude above NEI. Thermal detectors are superior in this respect.

Cooling

The response of certain quantum detectors can be extended well beyond the 7 micron uncooled limit with the aid of cryogenic refrigeration techniques. Several types and classes of cryogenic refrigerators are in common usage, although a variety of efficiencies are encountered. A useful indicator of the efficiency of a refrigeration system is provided by its coefficient of performance (COP), which is defined as the ratio of the cooling power of a system to the input power from all sources.

Open cycle refrigerators do not provide any reuse of the available coolant. Typical systems include *liquid-transfer*, including a coolant reservoir and feed line to the detector, *Joule-Thomson*, employing a Joule-Thomson cryostat, *solid-refrigerant*, placed in good thermal contact with the detector, and *radiative-transfer*, for use in space vehicles.

Closed cycle refrigeration offers a more efficient usage of the available coolant although involving a greater power consumption. The open cycle Joule-Thomson system may be combined with a compressor to repressurize the gas leaving the cryostat, thus forming an efficient closed cycle system (COP = 1/100 for refrigeration temperature = $77^{\circ}K$). Other closed cycle systems include Claude refrigerators (COP = 1/50 @ $40^{\circ}K$, COP = 1/100 @ $20^{\circ}K$, COP = 1/200 @ $4.2^{\circ}K$), and Stirling refrigerators (COP = 1/30 @ $77^{\circ}K$), although microphonics represent a serious noise problem in both types.

In the published literature, little consideration has been given to the effect of the refrigeration system on total system performance. Oscillations or variations in temperature, which may be inherent in the cooling system or caused by variations in irradiance or detector bias current, alter the detector characteristics. Also, noise is often introduced by the operation of the refrigeration device. For a Stirling refrigerator the noise generated when using a Mercury doped Germanium detector is at least double that generated by the detector alone (for chopping frequencies below 400 Hz or above 2000Hz).

Signal Processing

The output from any detector is a low level signal

which must be amplified before it becomes suitable for display or control of a recording device. A small preamplifier is located near the detector to provide a suitably high signal level for transmission along shielded cable to the remainder of the signal processing electronics. Additional amplification, bandwidth limiting, and detection are necessary before display is possible. For multielement detectors, time multiplexing circuitry is also required. Conventional AGC circuitry, logarithmic amplifiers, or AGC connected to detector bias circuitry to reduce responsivity, are used to provide the necessary wide dynamic range required by many systems to accomodate changes in signal level on the order of 10^4 or 10^6.

The most critical element of the signal processing equipment is the preamplifier. It must have a low noise figure and a minimum voltage gain of 10 to insure that the noise contributed by succeeding stages is negligible; a gain of 30 to 100 is desirable. AGC is not included in the preamplifier in order to maintain the lowest possible noise figure. An output impedance on the order of 100 to 1000Ω minimizes pickup in low-noise shielded cables.

Preamplifiers using vacuum tubes introduce Johnson and shot noise to the detector signal. Although maximum power transfer occurs when the equivalent resistance of the detector circuit (R_s) equals the input resistance of

the preamplifier, (R_g), a lower noise factor can be obtained by prudent selection of R_s. Assuming 1/f noise is negligible, the noise factor is given by

$$F = 1 + \frac{R_s}{R_g} + \frac{R_{eq}}{R_s}\left(1 + \frac{R_s}{R_g}\right)^2 \qquad (II\text{-}20)$$

where: R_{eq} = equivalent noise resistance of the preamplifier

R_s = source resistance

R_g = grid resistance

For minimum noise factor, the optimum value for the source resistance is

$$R_{s_{opt}} = R_g\left(\frac{R_{eq}}{R_g + R_{eq}}\right)^{1/2} \qquad (II\text{-}21)$$

and the corresponding noise factor is

$$F_{min} = 1 + \frac{2R_{eq}}{R_g} + 2\left[\frac{R_{eq}}{R_g}\left(1 + \frac{R_{eq}}{R_g}\right)\right]^{1/2} \qquad (II\text{-}22)$$

The equivalent noise resistance of a triode above 1000 Hz is

$$R_{eq_t} = \frac{2.5}{g_m} \qquad (II-23)$$

where: g_m = grid-plate transconductance

For pentodes,

$$R_{eq_p} = R_{eq_t}\left(1 + \frac{8I_c}{g_{m_p}}\right) \qquad (II-24)$$

where: Ic = screen grid current

p,t = subscripts indicating corresponding quantities for the tube connected as a pentode or a triode, respectively

Little information is available in the unclassified literature concerning the performance of transistors in infrared applications. The noise factor increases at low frequencies due to 1/f noise but is constant above 500 Hz for high gain planar transistors. In general, a low noise factor also requires a small base spreading resistance, short circuit common base current gain α approximately equal to unity, high short circuit current gain 3 dB cutoff frequency, and low emitter current. The optimum

source resistance ranges from 100Ω to 10,000Ω and results in a noise figure near 1 dB over a wide frequency range.

System Performance

Exact expressions for the performance of composite infrared systems are, in general, very difficult to evaluate but sufficiently accurate engineering approximations have been formulated. The most popular approximations involve the replacement of wavelength dependent quantities with their average over the spectral region of interest. For example, the generalized range equation for an infrared system limited by detector noise, and viewing an unresolved target (that is, one that does not fill the instantaneous field of view) has been given by Hudson [18]

$$R = \left[\frac{\pi D_o (NA) D^* J \tau_a \tau_o}{2(\omega \Delta f)^{1/2} (V_s/V_n)}\right]^{1/2} \qquad (II\text{-}25)$$

where: D_o = diameter of the collecting aperture

(NA) = numerical aperture of the optics

J = radiant intensity of the target over the spectral bandpass of the sensor

τ_a = average transmittance of the atmosphere over the spectral bandpass

τ_o = average transmittance of the optics over the spectral bandpass

An idealized maximum range, R_o, occurs when V_s/V_n equals unity for which case the irradiance at the detector becomes the noise equivalent irradiance NEI, given by

$$NEI = \frac{2(\omega \Delta f)^{1/2}}{\pi D_o (NA) D^* \tau_o} \qquad (II-26)$$

Similarly, the idealized maximum range for a background limited infrared system employing a photoconductive detector and a cooled shield to limit the detector view to a half angle Θ is

$$R_o = \left[\frac{\pi D_o J \tau_a \tau_o s \lambda}{4hc} \left(\frac{\eta_q}{Q_b \omega \Delta f} \right)^{1/2} \right]^{1/2} \qquad (II-27)$$

where: S = relative detector spectral response averaged over the system spectral bandpass

η_q = detector quantum efficiency

Q_b = background flux

The generalized range equation can in principle be applied to any type of infrared system although certain modifications may be necessary. In this thesis, emphasis is on passive infrared systems with applications in remote sensing of environment: radiometers and line scan imagers.

For a radiometer viewing an unresolved target, the

apparent temperature is related to the system parameters by

$$T = \left[\frac{2R^2(\omega \Delta f)^{1/2}}{\sigma A_s D_o (NA) D^* \tau_a \tau_o} \left(\frac{V_s}{V_n}\right)\left(\frac{V_s}{V_p}\right) \right]^{1/4} \quad \text{(II-28)}$$

where: V_p = peak value of the signal voltage

A_s = area of the source

Although this expression does not give a number value for the performance of a radiometer, it does indicate the effect of various system parameters. Similarly, the apparent temperature of an extended source is given by

$$T = \left[\frac{2}{\sigma D_o (NA) D^* \tau_a \tau_o} \left(\frac{V_s}{V_n}\right)\left(\frac{V_s}{V_p}\right)\left(\frac{\Delta f}{\omega}\right)^{1/2} \right]^{1/4} \quad \text{(II-29)}$$

Line scan thermal mapping systems view targets which fill the instantaneous field of view at all times and the irradiance at the collecting aperature is independent of the distance to the target. System performance can be expressed in terms of a noise equivalent differential temperature (NEΔT) which is defined as the temperature differential between two adjacent target elements that produces a signal equal to the system noise. (The temperature differential is actually an apparent

temperature differential.) The noise equivalent irradiance given by

$$NEI = \frac{2}{D_o(NA)D^* \tau_o}\left(\frac{2\mathcal{V}}{\pi C v}\right)^{1/2} \qquad (II\text{-}30)$$

where: $\mathcal{V}$ = velocity to height ratio for the airborne platform

v = pulse visibility factor defined by Genoud [19]

$$V = \left(\frac{V_p}{V_{ss}}\right)^2 \frac{1}{\tau_d \Delta f} \qquad (II\text{-}31)$$

In this expression, V_{ss} is the idealized (no loss) output from the signal processor and τ_d is the detector dwell time expressed by

$$\tau_d = \frac{\omega C}{\dot{\Omega}} \qquad (II\text{-}32)$$

where: $\dot{\Omega}$ = scan rate

C = number of detector elements

ω = instantaneous field of view

2

The noise equivalent differential temperature is related to NEI by

$$NE\Delta T = \frac{NEI}{\omega \tau_a \Delta N} \qquad (II\text{-}33)$$

where: ΔN = differential radiance of the target which can be expressed using suitable engineering approximations (τ_a, τ_o, and s averaged over spectral bandpass):

$$\Delta N = \tau_a \tau_o s \left(\frac{\delta N_\lambda}{\delta T}\right) d\lambda \qquad (II\text{-}34)$$

Hudson [20] has compiled a table of values for the integral in II-34 for several atmospheric windows and target temperature of 300°K.

Klein [21] has introduced several performance indicators which prove useful in the evaluation of passive infrared line scanning systems. He has expanded on the specific detectivity D* as defined by Jones to refer to the detectivity of a detector viewing a hemispherical blackbody surround at 295°K.

$$D^* = \left(\frac{1}{g}\right)\left(\frac{\lambda_c}{hc}\right)\left(\frac{\eta_q}{\Phi_o}\right)^{1/2} \qquad (II\text{-}35)$$

where: g = characteristic of the type of detector ($g = 2$ for photoconductive, $g = \sqrt{2}$ for photovoltaic)

λ_c = cutoff wavelength for the detector

η_g = detector quantum efficiency

ϕ_o = photon flux density at the entrance aperture

Similarly, a specific noise-equivalent irradiance is defined

$$(NEI)^* = \frac{2[\omega \Delta f]^{1/2}}{\pi (D_o)(NA)\, \tau_o\, \eta_e\, \mathcal{D}^*} \qquad (II\text{-}36)$$

where: $\eta_e = V_p/V_s$

Incorporating Genoud's pulse visibility factor and a scanning efficiency η_s, reflecting coverage redundancies and waste motion,

$$(NEI)^* = \left[\frac{2}{\pi D_o (NA) \tau_o \mathcal{D}^*}\right]\left[\frac{\dot{\Omega}}{C \eta_s V}\right]^{1/2} \qquad (II\text{-}37)$$

This exhibits the dependence of system performance on scanning rate.

Noise equivalent irradiance is related to this specific NEI by

$$NEI = (NEI)^* \left(\frac{\Phi_b}{\Phi_o}\right)^{1/2} \qquad (II-38)$$

or

$$NEI = \left[\frac{2}{\pi D_o \tau_o \mathcal{D}^*}\right]\left[\frac{K_b K_r \dot{\Omega}}{C \eta_s V}\right] \qquad (II-39)$$

where: $K_b = Q_b/Q_o$, and K_r is the radiation shielding factor

This expression is valid under three assumptions, presuming photon limited noise characteristics: (1) no solar reflection, (2) background approximate a blackbody at T_b and (3) a cold shield, and a cold filter are employed.

Klein further introduced a figure of merit defined as

$$\varphi = \frac{\sqrt{\dot{\Omega}}}{(MDTD)} \qquad (II-40)$$

where MDTD is the minimum detectable temperature difference as imposed by system parameters. The figure of merit is expressed by

$$\mathcal{P} = [\sqrt{\eta_s V}\,\eta_o][D_o\sqrt{C}\,\mathcal{D}^{*}\tfrac{1}{2}]\left[\frac{\epsilon}{\sqrt{K_b K_r}}\left(\frac{\delta W_\lambda}{\delta T}\right)\right] \qquad \text{(II-41)}$$

where: ε = emissivity of the target

$(\partial W_\lambda / \partial T)$ = temp. rate of change of Planck's Law (A-1).

This expression according to Klein, "clearly identifies design parameters and target characteristics that determine the total system performance of contemporary radiation-shielded thermal mappers".

CHAPTER III

ELECTROMAGNETIC REFLECTION FROM TARGET SURFACES

The characteristics of remote sensing data are indicative of the total extra-sensory radiation situation, including contributions from three general types of sources: target, background, and intervening medium. The contribution by each source becomes involved in certain electromagnetic phenomena including generation, emission, absorption, and reflection. An understanding of this extra-sensory situation requires a knowledge of the past phenomenological history of the specific components involved. Accordingly, a theoretical investigation of the reflective scattering of radiation from rough surfaces is presented in this chapter.

General Scattering Problem

The scattering of electromagnetic waves from "rough" surfaces has been a topic of considerable interest in recent years. Significant contributions toward a general theory of scattering have been made by many scientists and mathematicians, although existing theories fail to completely explain experimental results. The complexity of existing theories and their inability to account for experimental data form the impetus for this chapter. The

approach presented is not the traditional method used to examine rough surface scattering, but is simplified by visualization of the physical situation. The scattering mechanism is examined by a method which may be strictly classified as a Kirchhoff approach, but is not concerned with the process of solving the boundary value problem. The Fresnel reflection coefficients, which represent the plane surface solution of the boundary value problem are assumed to be valid over small areas of a rough surface, allowing the calculation of directional reflectances in terms of the surface characteristics. In Chapter IV, the approach is modified to examine the emission from a rough surface.

The general problem associated with rough surface scattering is indicated in Figure III-1. A quantity of electromagnetic energy, incident from the direction $\bar{r}_i$, onto an elemental area of surface dS, is redirected into various directions depending on the surface roughness characteristics. Traditionally, the ratio of the scattered electric field into a particular direction $\bar{r}_s$, to the incident electric field from the direction $\bar{r}_i$, is referred to as the scattering coefficient, γ_{si}, which is expressed by

$$\gamma_{VV} = \frac{E_V^s}{E_V^i}$$

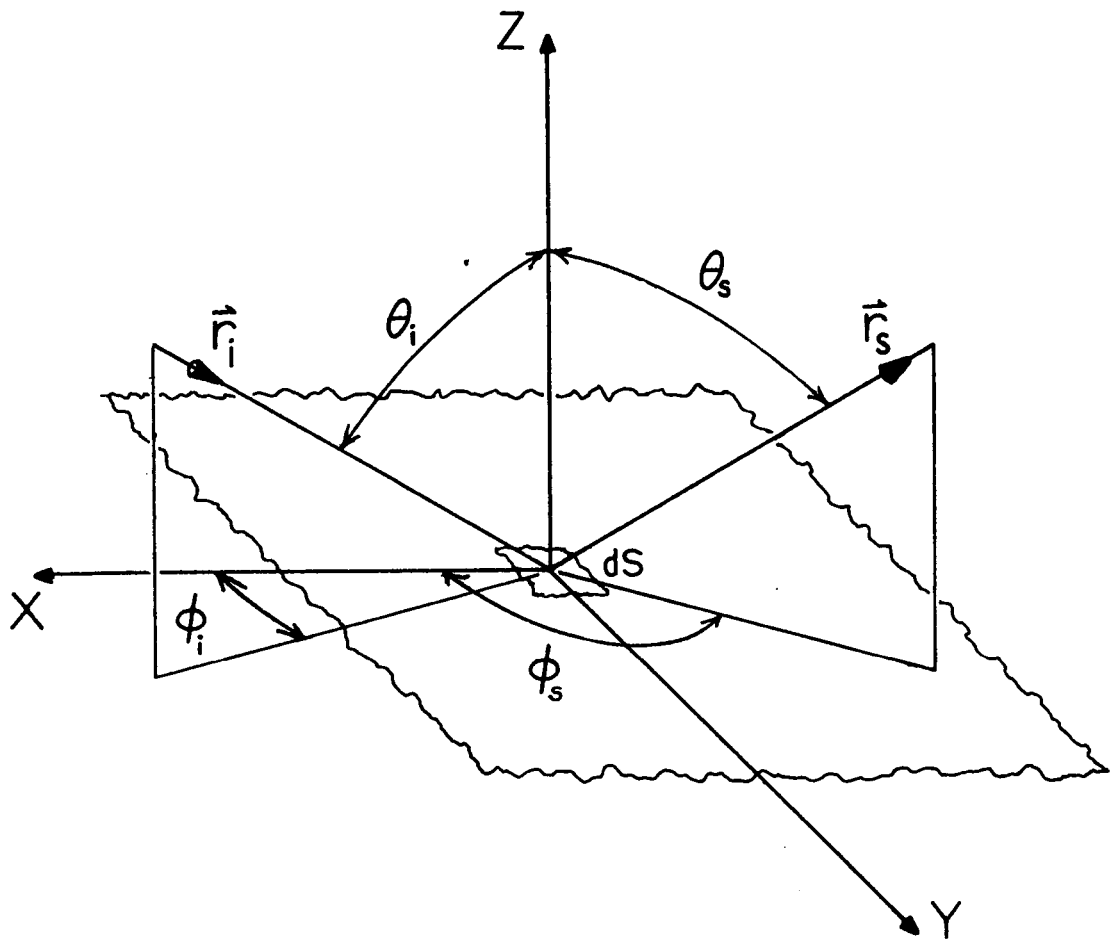

Figure III-1

General Scattering Geometry

$$\gamma_{HH} = \frac{E_H^s}{E_H^i}$$

$$\gamma_{VH} = \frac{E_V^s}{E_H^i} \qquad \text{(III-1)}$$

$$\gamma_{HV} = \frac{E_H^s}{E_V^i}$$

where the subscripts V, H indicate vertical or horizontal polarization in relation to the mean coordinate system. For the scattering coefficients, the first subscript indicates the polarization of the scattered electric field, and the second indicates the polarization of the incident electric field; this notation follows that of Peake and Barrick [22]. The superscripts s, i, indicate scattered and incident fields respectively. In this chapter, expressions are derived for these scattering coefficients to insure that the present development is compatable with other work in the field.

Rough Surface Scattering Model

The general scattering problem as outlined, may be

examined in terms of the traditional concept of scattering coefficients. Each incident or reflected direction is indicated by its azimuth and zenith angles with respect to the mean coordinate system (Figure III-1, p. 58). Additionally, parameters delineating the surface characteristics are required to describe the total redirection of incident radiation energy.

Localized Parameters

Local surface normal. The element of surface dS is presumed to contain an "effective area" oriented such that the radiation incident from the direction (θ_i, ϕ_i) is specularly reflected into the direction (θ_s, ϕ_s). The effective area oriented in the proper direction is a function of the surface roughness and of the incident and scattering directions.

Each incident and scattered directional pair (r_i, r_s) implies the orientation of the effective surface area and its local normal, $\bar{n}$. The orientation of the local effective normal is described by its zenith and azimuth angles (θ_n, ϕ_n) with respect to the mean coordinate system (Figure III-2). The statistical properties of the surface may be described in terms of these angles, and other parameters of interest are related to the zenith and azimuth angles of $\bar{r}_i$, $\bar{r}_s$, and $\bar{n}$.

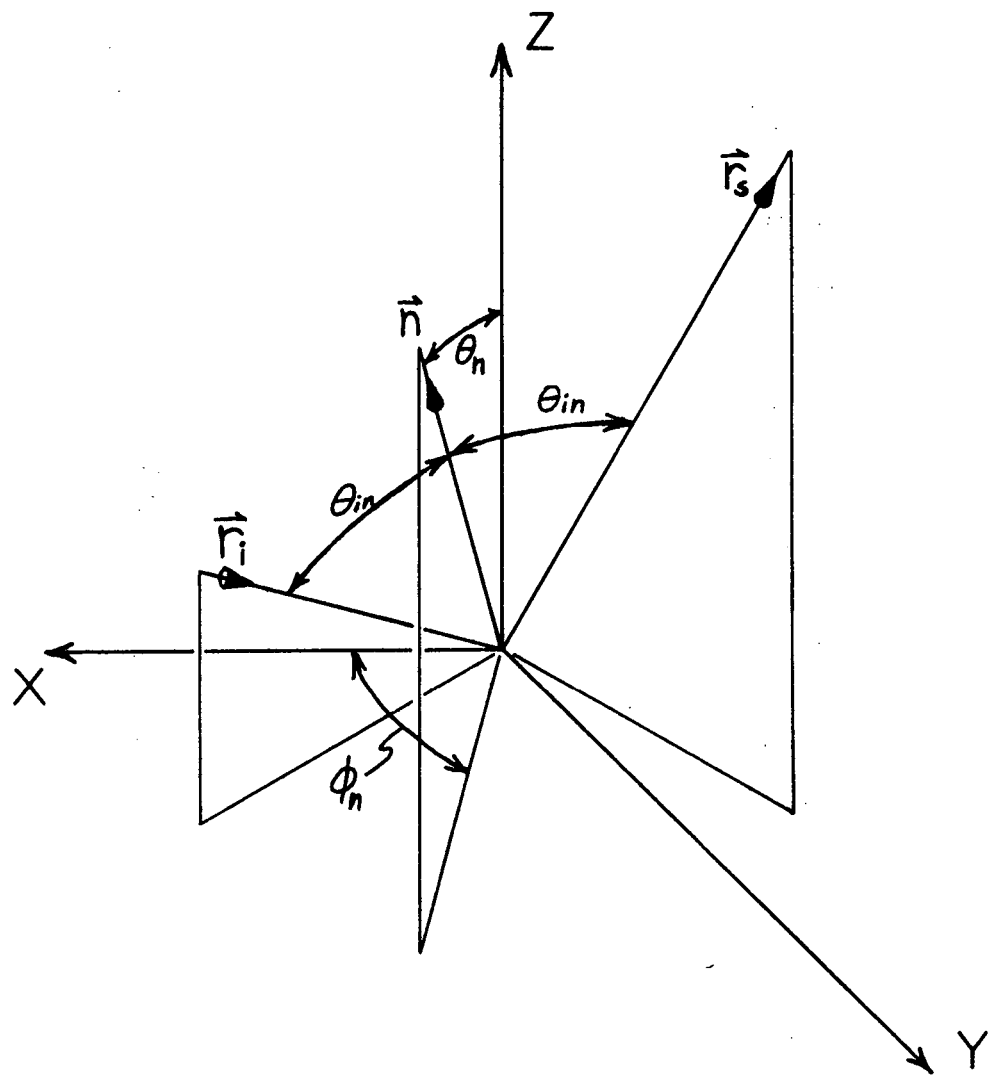

Figure III-2

Local Incidence Geometry

Local incidence angle. The local effective normal lies in the plane formed by $\bar{r}_i$, and $\bar{r}_s$, and bisects the angle between them in accordance with Snell's Law of reflection (Figure III-2, p.61). The angle, θ_{in}, between the local effective normal and either $\bar{r}_i$ or $\bar{r}_s$ is of significance in computation of the Fresnel reflection coefficients and is one half the angle between $\bar{r}_i$ and $\bar{r}_s$. Thus, determination of the local incidence angle may be accomplished by finding the angle between $\bar{r}_i$ and $\bar{r}_s$ and dividing by two.

A simple geometrical construction (Figure III-3) provides the basis for determination of the local incidence angle. According to the Law of Cosines for oblique spherical triangles [23], the angle between two radii ($\bar{r}_i$ and $\bar{r}_s$ in this case) is directly related to the angles between each one and a third radius ($\bar{k}$). The angle between the arcs a' and b', defined by (r_i, k) and (r_s, k) respectively on the unit sphere, is exactly equal to the angle between the projections of $\bar{r}_i$ and $\bar{r}_s$ on the x-y plane ($\phi_s - \phi_i$). The relationship is given by

$$\cos\theta_{is} = \cos\theta_s \cos\theta_i + \sin\theta_s \sin\theta_i \cos(\phi_s - \phi_i) \qquad \text{(III-2)}$$

The local incidence angle, θ_{in}, is given by one half of θ_{is}.

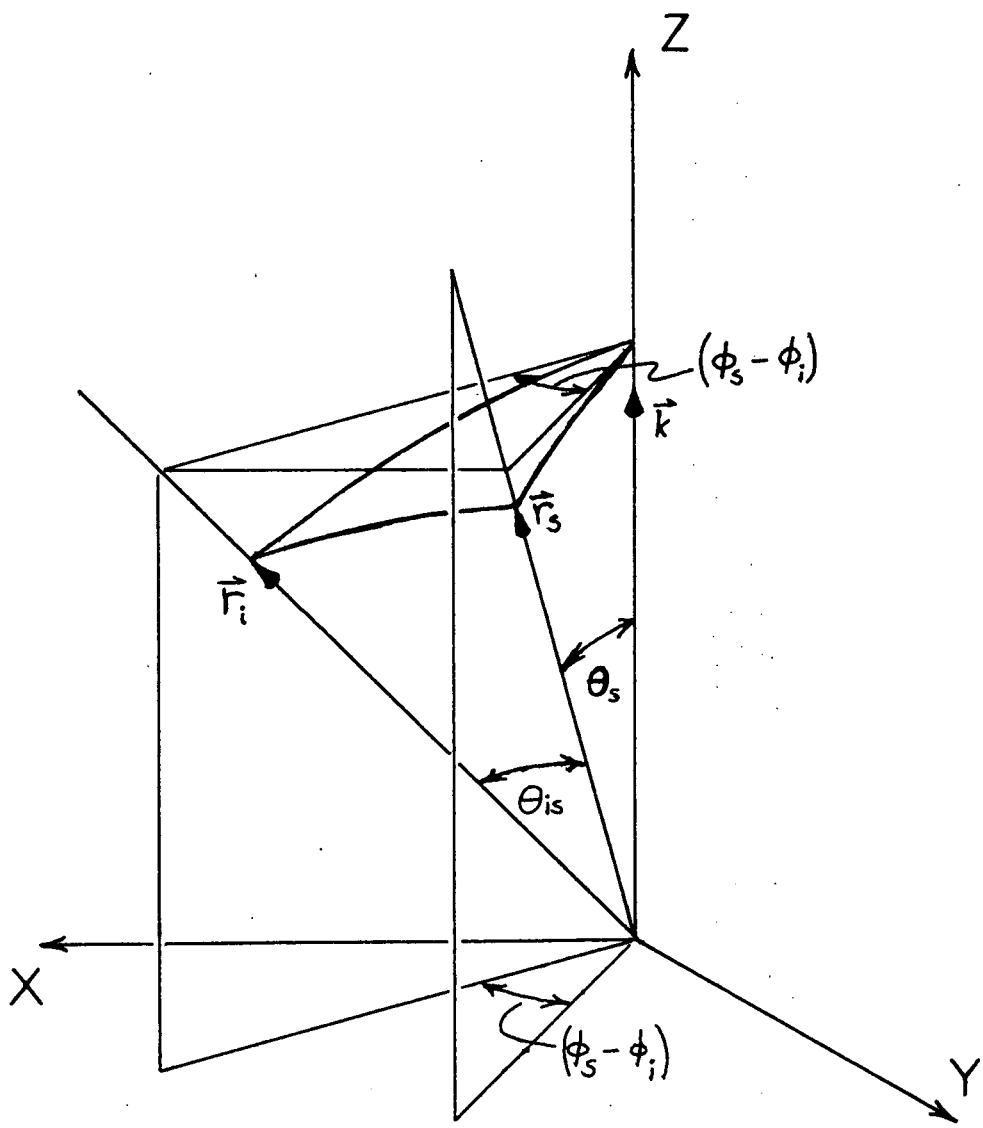

Figure III-3

Oblique Spherical Triangles

Local polarization. Incident radiation which is polarized vertical or horizontal in relation to the mean coordinate system appears to have vertical and horizontal components in relation to the local coordinates. The vertical and horizontal incident radiation may be transformed into locally vertical and horizontal components to conform to the definition of the Fresnel reflection coefficients.

Since the incident fields must be orthogonal to the incident direction of propagation, the locally vertical polarization direction can be represented by a simple rotation, α_i, of the mean vertical coordinate about the line of incidence (Figure III-4). The local polarization coordinates are oriented such that the local vertical coordinate lies in the local plane of incidence formed by $\bar{r}_i$ and $\bar{r}_s$. The angle of rotation, α_i, is obtainable in a manner similar to the method used to find the local incidence angle; using the Law of Cosines for sides of oblique spherical triangles, [24]

$$\cos \alpha_i = \frac{\cos \theta_s - \cos \theta_{is} \cos \theta_i}{\sin \theta_{is} \sin \theta_i} \qquad \text{(III-3)}$$

For incident radiation consisting of vertical and horizontal polarization components, the locally polarized

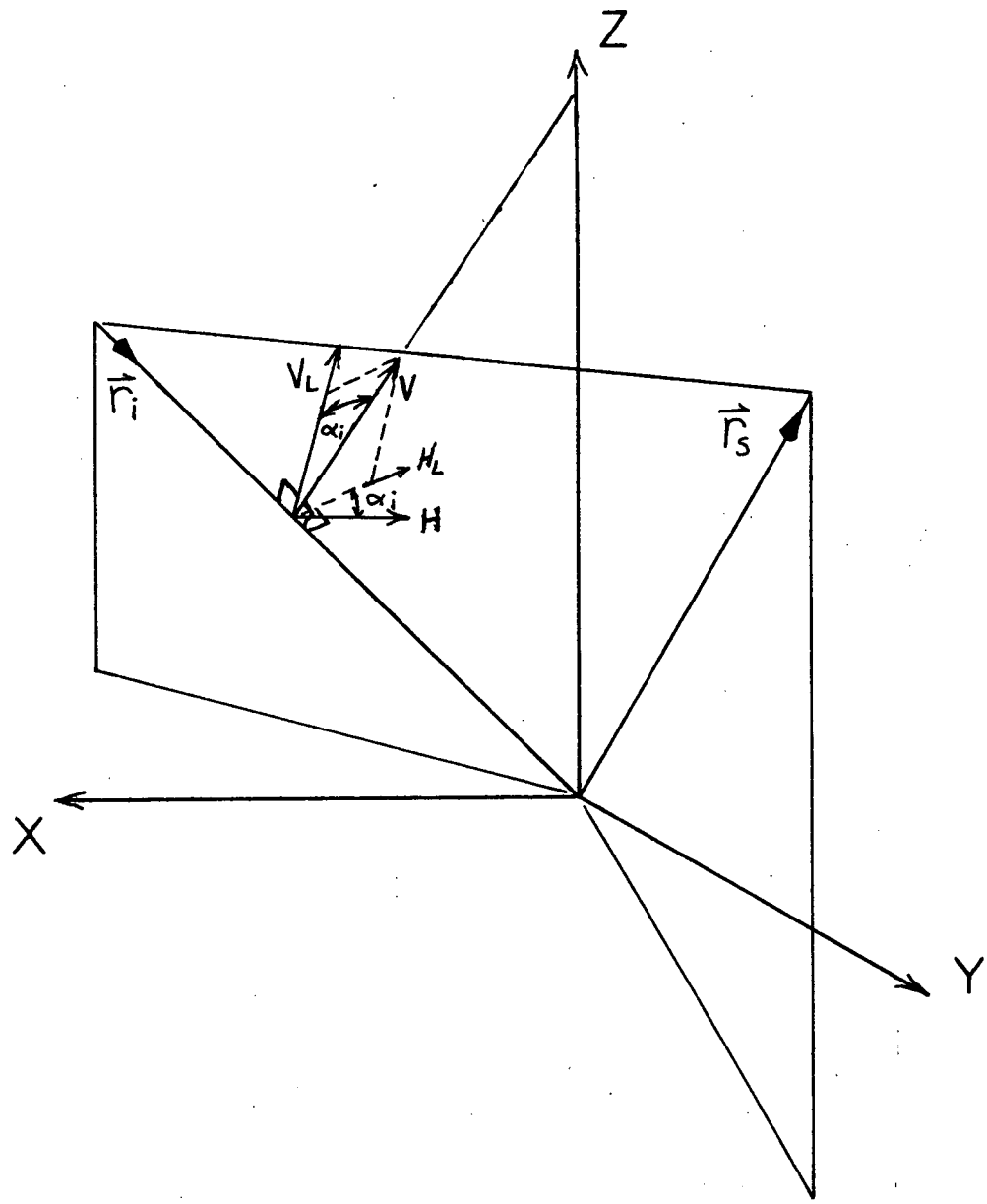

Figure III-4

Local Polarization

components are related by

$$E^i_{LV} = E^i_V \cos\alpha_i + E^i_H \sin\alpha_i$$

$$E^i_{LH} = E^i_H \cos\alpha_i - E^i_V \sin\alpha_i \qquad \text{(III-4)}$$

Here, the subscripts LV, LH indicate locally vertical and horizontal components respectively. The local scattered components into the direction $\bar{r}_s$, assuming validity of the tangent plane approximation is

$$E^s_{LV} = \rho_V E^i_{LV}$$

$$E^s_{LH} = \rho_H E^i_{LH} \qquad \text{(III-5)}$$

where ρ_V, ρ_H are the Fresnel reflection coefficients given by [25]

$$\rho_V = \frac{\eta_2 \cos\theta_2 - \eta_1 \cos\theta_{in}}{\eta_2 \cos\theta_2 + \eta_1 \cos\theta_{in}}$$

$$\text{(III-6)}$$

$$\rho_H = \frac{\eta_2 \cos\theta_{in} - \eta_1 \cos\theta_2}{\eta_2 \cos\theta_{in} + \eta_1 \cos\theta_2}$$

where $\eta_{1,2} = \frac{\mu_{1,2}}{\varepsilon_{1,2}}$ = intrinsic impedance of the upper, lower medium

$\theta_{in} = \frac{1}{2}\theta_{is}$ = local incidence angle

θ_2 = local angle of refraction (Figure III-5)

and from Snell's law [26]

$$\cos\theta_2 = \sqrt{1 - \left(\frac{n_1}{n_2}\right)^2 \sin\theta_{in}} \qquad (III-7)$$

where $n_{1,2} = \sqrt{\mu_{1,2}\,\varepsilon_{1,2}}$ = index of refraction of the upper, lower medium

The local polarization of the reflected components is related to the polarization coordinates of the reflected direction by a simple rotation, α_r, of coordinate axes about the line of reflection. This transformation is analagous to the rotation of incident polarization coordinates to obtain the local polarization. Therefore,

$$\cos\alpha_r = \frac{\cos\theta_i - \cos\theta_{is}\cos\theta_s}{\sin\theta_{is}\sin\theta_s} \qquad (III-8)$$

The scattered fields in the direction $\bar{r}_s$, are

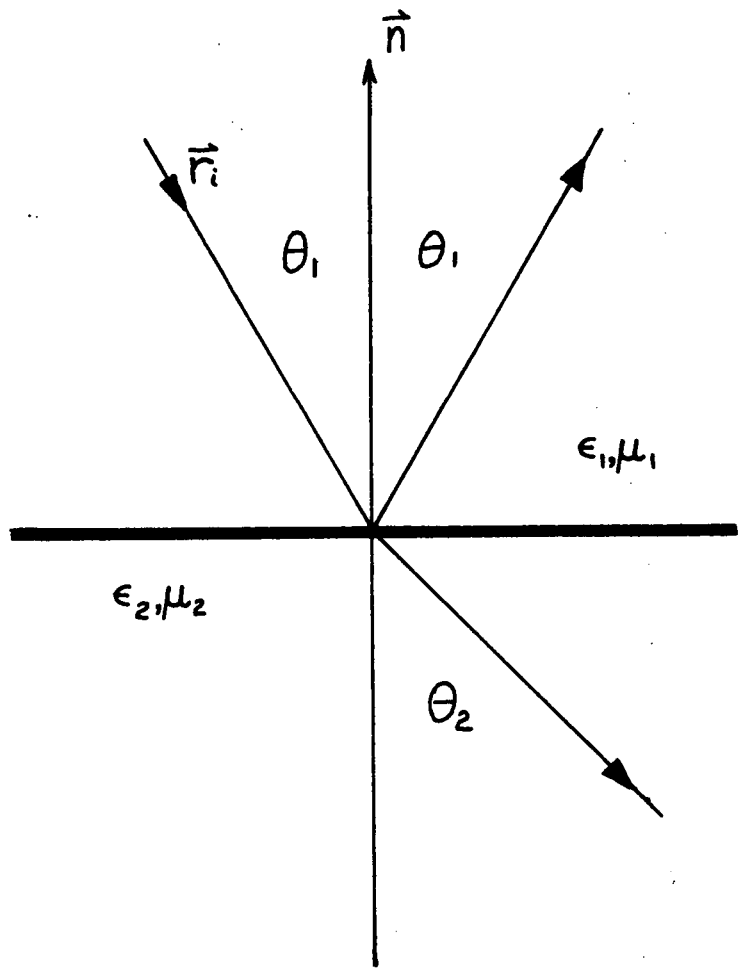

Figure III-5

External Specular Reflection
and Refraction Geometry

$$E_V^s = E_{LV}^s \cos\alpha_r - E_{LH}^s \sin\alpha_r$$

$$E_H^s = E_{LV}^s \sin\alpha_r + E_{LH}^s \cos\alpha_r \qquad \text{(III-9)}$$

Combining (III-4), (III-5), and (III-9), the scattered fields may be written:

$$E_V^s = \rho_V \left[E_V^i \cos\alpha_i + E_H^i \sin\alpha_i\right] \cos\alpha_r - \rho_H \left[E_H^i \cos\alpha_i - E_V^i \sin\alpha_i\right] \sin\alpha_r \qquad \text{(III-10)}$$

$$E_H^s = \rho_V \left[E_V^i \cos\alpha_i + E_H^i \sin\alpha_i\right] \sin\alpha_r + \rho_H \left[E_H^i \cos\alpha_i - E_V^i \sin\alpha_i\right] \cos\alpha_r$$

where the Fresnel reflection coefficients are given by (III-6) in conjunction with (III-2) and (III-7).

Scattering coefficients. The traditional scattering coefficients as defined by (III-1) are obtainable from (III-10);

$$\gamma_{VV} = \rho_V \cos\alpha_i \cos\alpha_r + \rho_H \sin\alpha_i \sin\alpha_r$$

$$\gamma_{HH} = \rho_V \sin\alpha_i \sin\alpha_r + \rho_H \cos\alpha_i \cos\alpha_r \qquad \text{(III-11)}$$

$$\gamma_{HV} = \rho_V \sin\alpha_i \cos\alpha_r - \rho_H \cos\alpha_i \sin\alpha_r$$

$$\gamma_{VH} = \rho_V \cos\alpha_i \sin\alpha_r - \rho_H \sin\alpha_i \cos\alpha_r$$

where ρ_V, ρ_H are the Fresnel reflection coefficients and α_i, α_r are the incident and reflected rotations of polarization coordinates into the local plane of incidence given by (III-3) and (III-8). If the incident and reflected directions are interchanged, the theorem of reciprocity is not violated by this formulation. These coefficients represent the transmission characteristics of plane elemental surfaces as a function of their orientation with respect to the mean coordinate system; they do not account for the relative quantities of effective area available for specular reflection for each incident and scattered directional pair (r_i, r_s).

Surface Model

Statistical parameters. The characteristics of the surface may be completely described by a surface height function of position on the mean coordinate plane;

$$Z = Z(x,y) \qquad \text{(III-12)}$$

From this approach, other authors have solved the boundary value problem at the surface to obtain expressions for the scattered fields under certain assumptions. In the remainder of this chapter the method of physical optics is applied to a general surface described by certain probability distribution functions.

The surface distribution of heights above the mean plane implies certain other spatial distributions which more readily facilitate the present method of solution. It will suffice to say that the function (III-12) is related to a spatial distribution of local normals, which is also sufficient to completely describe the surface characteristics.

Since the local normals are represented by their zenith and azimuth angles, measured in relation to the mean coordinate system, their statistical properties may be described by the statistics of their representative angles

θ_n, ϕ_n. The spatial distribution of local normals implies a probability density function of the random variables θ_n, ϕ_n. Following the notation of Papoulis, [27] the joint density for zenith and azimuth angles of the local normal is

$$f_{\theta\phi}(\theta_n, \phi_n) \qquad \text{(III-13)}$$

The marginal density of the azimuth random variable ϕ_n is assumed to be uniform and independent of the zenith random variable. Thus since ϕ_n may assume only values in the region $(0 \leq \phi_n \leq 2\pi)$; its' marginal density is given by

$$f_{\phi}(\phi_n) = \frac{1}{2\pi} \qquad (0 \leq \phi_n \leq 2\pi) \qquad \text{(III-14)}$$

and the joint density becomes:

$$f_{\theta\phi}(\theta_n, \phi_n) = \frac{f_{\theta}(\theta_n)}{2\pi} \qquad \text{(III-15)}$$

This density function will serve to describe the surface characteristics of various random rough surfaces, and is related to the specific factors of interest in for-

mulation of the scattering problem.

Effective area. Each element of actual surface area, dS, may be associated with a corresponding projection onto the mean coordinate plane, dA. A certain fraction, β, of dS is oriented in the proper position to permit radiation from the direction $\bar{r}_i$ to be redirected into the direction $\bar{r}_s$. The effective area for reflection from $\bar{r}_i$ into $\bar{r}_s$, within a solid angle $d\Omega$, is

$$dA_{eff} = \beta \, dS \qquad \text{(III-16)}$$

where β is the "coefficient of effective area". The element of actual surface dS is a function of the surface roughness, therefore

$$dS = \delta \, dA \qquad \text{(III-17)}$$

where δ is the "surface roughness factor".

The coefficient of effective area, β, and the surface roughness factor, δ, are related to the statistical distribution of surface normals. The joint density function for the zenith and azimuth random variables defines the statistics of the surface normals and is given by (III-15).

The zenith distribution of surface normals may be of any form, depending only on the surface state and will serve to describe the surface normal statistics.

The coefficient of effective area, β, is related to the probability density for the surface normals. The probability that the surface normal is oriented in the proper direction, within the limits $d\theta$, $d\phi$ is

$$\frac{1}{2\pi} f_\theta(\theta_n)\, d\theta_n\, d\phi_n \qquad \text{(III-18)}$$

In spherical coordinates a solid angle bounded by $d\theta$, $d\phi$ is defined

$$d\Omega = \sin\theta \; d\theta \, d\phi \qquad \text{(III-19)}$$

Thus, the probability that the surface normal is oriented within $d\Omega$ is

$$\frac{f_\theta(\theta_n)}{2\pi \sin\theta}\, d\Omega \qquad \text{(III-20)}$$

The coefficient of effective area is

$$\beta = \frac{f_\theta(\theta_n)}{2\pi \sin \theta_n} \qquad \text{(III-21)}$$

This represents the fraction of total surface oriented within a unit solid angle about a particular direction. The projection of this element of surface onto the mean plane is

$$\frac{f_\theta(\theta_n) \cos \theta_n}{2\pi \sin \theta_n}$$

The total effect of all orientations is obtained by integration over the hemisphere

$$\frac{dA}{dS} = \frac{1}{\delta} = \int \frac{f_\theta(\theta_n) \cos \theta_n}{2\pi \sin \theta_n} \, d\Omega$$

Rearranging and integrating over the azimuth variable

$$\delta = \frac{1}{\int_0^{\pi/2} f_\theta(\theta_n) \cos \theta_n \, d\theta_n} \qquad \text{(III-22)}$$

Combining (III-16) and (III-17),

$$dA_{eff} = \beta \delta \, dA \qquad \text{(III-23)}$$

Substituting (III-21) and (III-22),

$$dA_{eff} = \frac{f_\theta(\theta_n)}{2\pi \sin\theta_n \int_0^{\pi/2} f_\theta(\theta_n) \cos\theta_n \, d\theta_n} dA \qquad \text{(III-24)}$$

which expresses the quantity of effective area available for specular reflection from (θ_i, ϕ_i) into (θ_s, ϕ_s) as a function of the surface parameters.

Phase Interference

The present formulation has, until now, neglected the phase interference due to different path lengths for the incident radiation reflected from different elements of effective area. In Appendix B, it is shown that there is no time average phase interaction of scattered fields due to different path lengths if the incident radiation is randomly phased.

Power Scattering Coefficients

The specific situation involving the scattering of

background radiation may be treated assuming that the incident background radiation is randomly phased. The incident goniometric polarized irradiance may be written using Poynting's theorem,

$$\vec{I}_{\lambda V} = \vec{E}^{i}_{V} \times \vec{H}^{i}_{V}$$

$$\vec{I}_{\lambda H} = \vec{E}^{i}_{H} \times \vec{H}^{i}_{H} \qquad \text{(III-25)}$$

where $I_{\lambda V}$ and $I_{\lambda H}$ are the vertical and horizontal components of the incident goniometric irradiance and E^{i}_{V}, E^{i}_{H}, H^{i}_{V}, H^{i}_{H} are the incident electric and magnetic fields from the direction (θ_i, ϕ_i). Of this irradiance a certain fraction falls on the effective area and is subsequently available for specular reflection into the direction (θ_s, ϕ_s). The fraction is expressed:

$$\vec{I}^{\,eff}_{\lambda V} = \frac{\cos\theta_i}{\beta\delta\cos\theta_{in}}\,\vec{I}_{\lambda V}$$

$$\vec{I}^{\,eff}_{\lambda H} = \frac{\cos\theta_i}{\beta\delta\cos\theta_{in}}\,\vec{I}_{\lambda H} \qquad \text{(III-26)}$$

and represents the irradiance from (θ_i, ϕ_i) which falls on the effective area.

The effective scattered polarized radiance into (θ_s, ϕ_s) from (θ_i, ϕ_i) can be written

$$\vec{N}_{\lambda V} = \vec{E}^{s}_{V} \times \vec{H}^{s}_{V}$$

$$\vec{N}_{\lambda H} = \vec{E}^{s}_{H} \times \vec{H}^{s}_{H} \qquad \text{(III-27)}$$

where $N_{\lambda V}$ and $N_{\lambda H}$ are the vertical and horizontal components of the scattered radiance and E^{s}_{V}, E^{s}_{H}, H^{s}_{V}, H^{s}_{H} are the effective scattered fields.

The effective incident and reflected fields are related by the scattering coefficients (III-11), therefore the scattered polarized radiance becomes

$$\vec{N}_{\lambda V} = (\gamma_{VV}\vec{E}^{i}_{V} + \gamma_{HV}\vec{E}^{i}_{H}) \times (\gamma_{VV}\vec{H}^{i}_{V} + \gamma_{HV}\vec{H}^{i}_{H})$$

$$\vec{N}_{\lambda H} = (\gamma_{HH}\vec{E}^{i}_{H} + \gamma_{VH}\vec{E}^{i}_{V}) \times (\gamma_{HH}\vec{H}^{i}_{H} + \gamma_{VH}\vec{H}^{i}_{V}) \qquad \text{(III-28)}$$

Expanding the cross products and realizing

$$\vec{E}^{i}_{V} \times \vec{H}^{i}_{H} = \vec{E}^{i}_{H} \times \vec{H}^{i}_{V} = \vec{O}$$

gives

$$\vec{N}_{\lambda V} = \gamma_{VV}^2(\vec{E}_V^i \times \vec{H}_V^i) + \gamma_{HV}^2(\vec{E}_H^i \times \vec{H}_H^i)$$

$$\vec{N}_{\lambda H} = \gamma_{HH}^2(\vec{E}_H^i \times \vec{H}_H^i) + \gamma_{VH}^2(\vec{E}_V^i \times \vec{H}_V^i) \qquad \text{(III-29)}$$

where the cross products represent the effective irradiance and are given by (III-26). Substituting (III-26) into (III-29),

$$N_{\lambda V} = \frac{\cos\theta_i}{\beta\delta\cos\theta_{in}}\left(\gamma_{VV}^2 I_{\lambda V} + \gamma_{HV}^2 I_{\lambda H}\right)$$

$$N_{\lambda H} = \frac{\cos\theta_i}{\beta\delta\cos\theta_{in}}\left(\gamma_{HH}^2 I_{\lambda H} + \gamma_{VH}^2 I_{\lambda V}\right) \qquad \text{(III-30)}$$

where $(\beta\delta)$ is expressed by (III-23) and (III-24) and the scattering coefficients are given by (III-11).

It is instructive to view the reduction of (III-30) for the smooth surface case. The density function for local normals $f_{\theta\phi}(\theta_n, \phi_n)$ becomes a density function for zenith angle only $f_\theta(\theta_n)$ which is an impulse at $(\theta = 0)$. The coefficient of effective area β becomes

$$\beta = \frac{f_\theta(\theta_n)}{\text{SIN}\,\theta_n}$$

and the limit as $\theta \to 0$ is found, using L' Hospitals' rule

$$\beta = 1$$

The surface roughness factor reduces to

$$\delta = 1$$

and

$$\cos\theta_i = \cos\theta_{in}$$

The scattering coefficients reduce as follows

$$\gamma_{VV} = \rho_V$$

$$\gamma_{HH} = \rho_H$$

$$\gamma_{HV} = \gamma_{VH} = 0$$

Therefore Equation (III-30) becomes for a smooth surface

$$N_{\lambda V} = \rho_V^2 \, I_{\lambda V}$$

$$N_{\lambda H} = \rho_H^2 \, I_{\lambda H} \qquad \text{(III-31)}$$

which is the correct result.

CHAPTER IV

GENERATION AND EMISSION OF THERMAL RADIATION

The radiation component of primary importance in passive sensing is the thermal radiation emission from the target. It is the predominant carrier of target information, although existing data interpretation techniques are unable to extract a majority of the information conveyed. This inability to accurately interpret data characteristics in terms of the various extra-sensory variables is largely a result of the absence of a theoretical model for the extra-sensory situation. In response to this data interpretation problem, this chapter provides the basis for a general theory of the thermal radiation emission.

Thermal Radiation Generation

The blackbody radiation laws presented in Appendix A are based on certain assumptions about the physical nature or radiating material. The assumptions are specifically noted in Planck's original derivation [28] and are presented in the course of this section.

Fundamental Concept

An attempt to describe the various radiation charac-

teristics of materials, logically begins by considering the actual source of the radiation emerging from the surface. The ultimate source is, of course, the atoms and molecules which comprise the material, however, a microscopic formulation of radiation characteristics is not manageable. Therefore, following Planck, consider a small volume element of the material which encompasses a sufficient quantity of elementary radiation sources such that homogeneity may be assumed (Figure IV-1). The radiative power emitted by the volume element is proportional to the volume and uniform in all directions, assuming the material is isotropic and in a state of thermal equilibrium; thermal equilibrium in this instance indicates zero temperature gradient throughout the material.

It naturally follows that the radiation propagates throughout the medium, interacting with other volume elements, and impinging upon the boundary at the surface where reflection and transmission occur. Obviously, the reflected component remains within the material, while the transmitted component escapes the surface (Figure IV-2). A basic premise of this chapter is that the transmitted component of the internal radiation is precisely the natural radiation emission from the material, as it certainly must be.

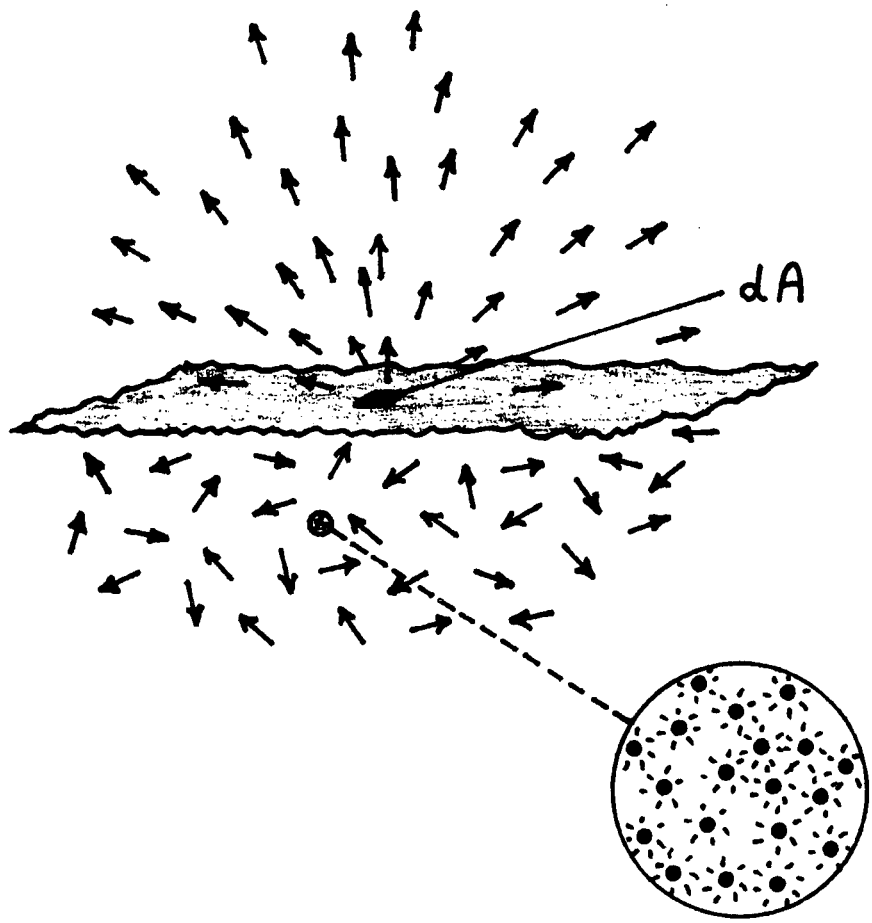

Figure IV-1

Generation and Emission of Thermal Radiation

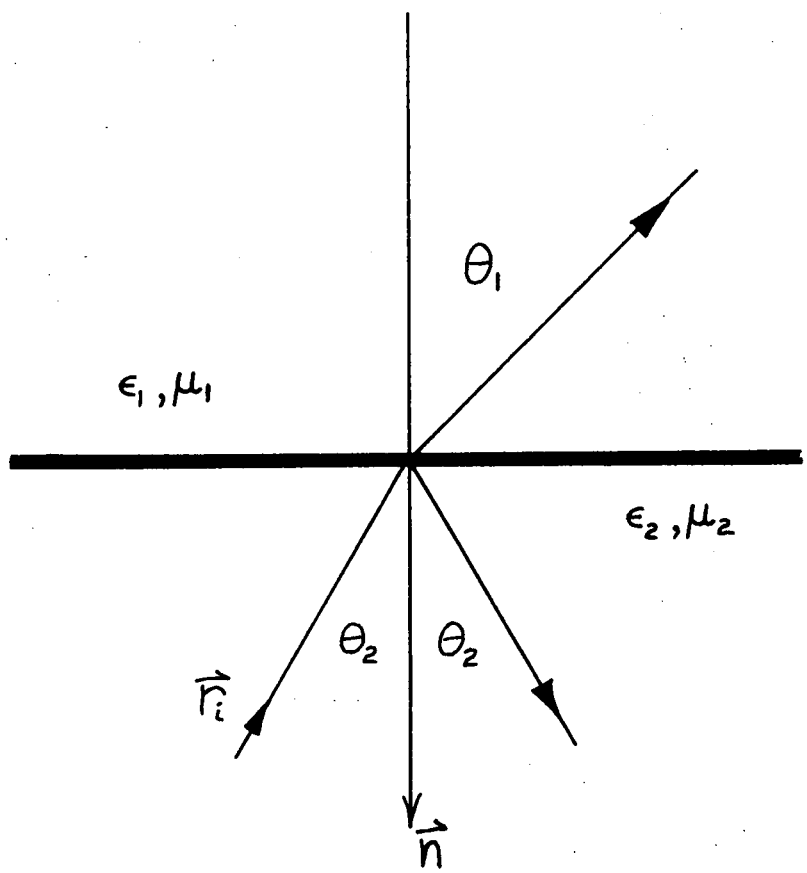

Figure IV-2

Internal Specular Reflection
and Refraction Geometry

Internal Radiation Characteristics

Application of the fundamental concept to describe the emission characteristics of an object requires a knowledge of the radiation properties within the material. Although these are not known specifically, under the given assumptions certain characteristics of internal radiation may be noted. For a homogeneous, isotropic medium in a state of thermodynamic equilibrium, the radiation flux at any location may be assumed to have perfectly random direction, polarization, and phase. From this assumption, the internal radiation incident upon the boundary is of the same random nature, and the radiative characteristics above the surface are then obtainable in terms of the transmission characteristics of the boundary. Alternatively, if the radiative characteristics above a surface are known, the internal radiation situation may be determined.

Basic radiation theory is based on theoretical objects (blackbodies) whose radiation characteristics are such that all radiation incident is absorbed (none reflected) and reradiated. They are described as perfect absorbers and radiators (Appendix A). The concept of perfect absorption and radiation indicates that the transmission of radiation energy across the boundary is complete for any direction or polarization. Thus, it is a simple matter to infer the internal irradiance characteristics of a blackbody.

The radiant emittance of a blackbody is described by Planck's Law (A-1,p.125), and is related to blackbody radiance by (A-9,p.129). Since for a blackbody, the transmission of radiation is complete for any direction, and subsurface spectral goniometric irradiance at any zenith angle equals the spectral radiance at the zenith angle;

$$I^b_{\lambda 2} = N^b_\lambda = \frac{1}{\pi} W^b_\lambda \qquad \text{(IV-1)}$$

Here, the subscript, 2, indicates subsurface. It should be noted that this expression also describes the radiation situation throughout the blackbody since it represents the spectral goniometric irradiance on any plane area internal to the blackbody.

Blackbody internal spectral goniometric volume density of radiation energy is related to the subsurface spectral goniometric irradiance by the velocity of propagation in the blackbody material

$$\vec{U}^b_{\lambda\Omega} = \frac{1}{v^b_p} \vec{I}^b_\lambda = \sqrt{\mu^b \epsilon^b}\, \vec{I}^b_\lambda \qquad \text{(IV-2)}$$

The internal spectral volume density of radiation energy is thus,

$$U_\lambda^b = 4\pi \sqrt{\mu^b \epsilon^b}\, I_\lambda^b \qquad \text{(IV-3)}$$

since independence of direction can be assumed without error. Similarly, for a physical material,

$$\vec{U}_{\lambda\Omega} = \sqrt{\mu\epsilon}\, \vec{I}_\lambda \qquad \text{(IV-4)}$$

and if thermodynamic equilibrium exists in a homogeneous isotropic material, independence of direction is assumed. Thus

$$U_\lambda = 4\pi \sqrt{\mu\epsilon}\, I_\lambda \qquad \text{(IV-5)}$$

exactly as given by Planck [29].

An interesting question arises: what is the velocity of propagation in a blackbody? The answer is not clear since the velocity may have any value approaching and including the speed of light. This is a result of the perfect absorption and emission characteristics of a blackbody. Complete transmission of energy at the surface of a black-

body requires that its electrical properties assume the values characteristic of the medium in which it is placed. Thus a blackbody provides a convenient reference and may be assumed to allow any velocity of propagation ($\leq c$).

The internal radiation density of real materials can be related to the internal radiation density of a blackbody at the same temperature. The spectral emissivity, ϵ_λ, of the real material is defined in Appendix A as the ratio of the internal volume density of spectral radiation energy of a material to that of a blackbody at the same temperature;

$$\epsilon_\lambda = \frac{U_\lambda}{U_\lambda^b} \qquad \text{(IV-6)}$$

The emissivity is a quality factor expressing a material's ability to approximate blackbody radiation characteristics internally, and is related to the possible energy transitions on the atomic scale for the specific material, in addition to the spatial density of potential sources of radiation.

Combining (IV-1), (IV-3), (IV-5), and (IV-6), the subsurface spectral goniometric irradiance can be related to the spectral radiant emittance of a blackbody whose permeability and permittivity exactly equal those of the

material, since a blackbody may exhibit any velocity of propagation;

$$I_{\lambda 2} = \frac{\epsilon_\lambda}{\pi} W_\lambda^b \qquad (IV-7)$$

The blackbody spectral radiant emittance, W_λ^b is given by (A-1, p. 125), and E_λ may be determined experimentally with the aid of the development presented in the remaining sections of this chapter.

Peake's Method

The angular dependence of radiation emission from a general surface has been formulated by Peake [30] on the basis of thermodynamic considerations. The rationale is straightforward; for a material in thermodynamic equilibrium with its surroundings, the radiation power emitted equals the radiation power absorbed, according to Kirchhoff's Law. The total power absorbed or emitted may be written

$$P_a = P_e = P_i - P_r \qquad (IV-8)$$

where: P_a = absorbed power

P_e = emitted power

P_i = incident power

P_r = reflected power

For a homogeneous, isotropic material in thermodynamic equilibrium, Kirchhoff's Law may be generalized for spectral, polarized, radiance and goniometric irradiance. Generalizing (IV-8) gives

$$N^e_{\lambda V} = I^i_{\lambda V} - N^r_{\lambda V}$$

$$N_{\lambda H} = I^i_{\lambda H} - N^r_{\lambda H} \qquad \text{(IV-9)}$$

where the subscripts V,H represent vertical or horizontal polarization components respectively and the superscripts e, i, and r indicate emitted, incident, and reflected radiance or goniometric irradiance respectively. (The radiometric terminology is defined in Appendix A).

The instantaneous power transferred by electromagnetic radiation is given by Poyting's theorem

$$\vec{P} = \vec{E} \times \vec{H}$$

where the units are watts per unit area. Extending this relationship to goniometric quantities, the instantaneous radiance may be written in terms of the spectral reflected

polarized goniometric fields;

$$\vec{N}^{r}_{\lambda V} = \vec{E}^{r}_{\lambda \Omega V} \times \vec{H}^{r}_{\lambda \Omega V}$$

$$\vec{N}^{r}_{\lambda H} = \vec{E}^{r}_{\lambda \Omega H} \times \vec{H}^{r}_{\lambda \Omega H} \qquad \text{(IV-10)}$$

where the subscript Ω indicates goniometric fields.

Using the Fresnel reflection coefficients, (IV-10) may be written

$$\vec{N}^{r}_{\lambda V} = \rho_V \vec{E}^{i}_{\lambda \Omega V} \times \rho_V \vec{H}^{i}_{\lambda \Omega V}$$

$$\vec{N}^{r}_{\lambda H} = \rho_H \vec{E}^{i}_{\lambda \Omega H} \times \rho_H \vec{H}^{i}_{\lambda \Omega H} \qquad \text{(IV-11)}$$

Similarly, the incident polarized spectral goniometric irradiance components are:

$$\vec{I}^{i}_{\lambda V} = \vec{E}^{i}_{\lambda \Omega V} \times \vec{H}^{i}_{\lambda \Omega V}$$

$$\vec{I}^{i}_{\lambda H} = \vec{E}^{i}_{\lambda \Omega H} \times \vec{H}^{i}_{\lambda \Omega H} \qquad \text{(IV-12)}$$

Combining (IV-9), (IV-11), and (IV-12),

$$\vec{N}^{e}_{\lambda V} = (1 - \rho_V^2)\, \vec{I}^{i}_{\lambda V}$$

$$N^{e}_{\lambda H} = (1 - \rho_H^2)\, I^{i}_{\lambda H} \qquad \text{(IV-13)}$$

These equations describe the angular dependence of polarized radiation emission from a smooth surface according to Peake. The Fresnel reflection coefficients are given by[31]

$$\rho_V = \frac{\eta_2 \cos\theta_2 - \eta_1 \cos\theta_1}{\eta_2 \cos\theta_2 + \eta_1 \cos\theta_1}$$

$$\rho_H = \frac{\eta_2 \cos\theta_1 - \eta_1 \cos\theta_2}{\eta_2 \cos\theta_1 + \eta_1 \cos\theta_2} \qquad \text{(IV-14)}$$

where: η_1, η_2 = intrinsic impedances of the two media ($\sqrt{\mu/\varepsilon}$)

θ_1, θ_2 = angles of incidence, refraction (Figure IV-3).

From Snells' Law [32]

$$\cos\theta_2 = \sqrt{1 - \left(\frac{n_1}{n_2}\right) \sin^2\theta_1} \qquad \text{(IV-15)}$$

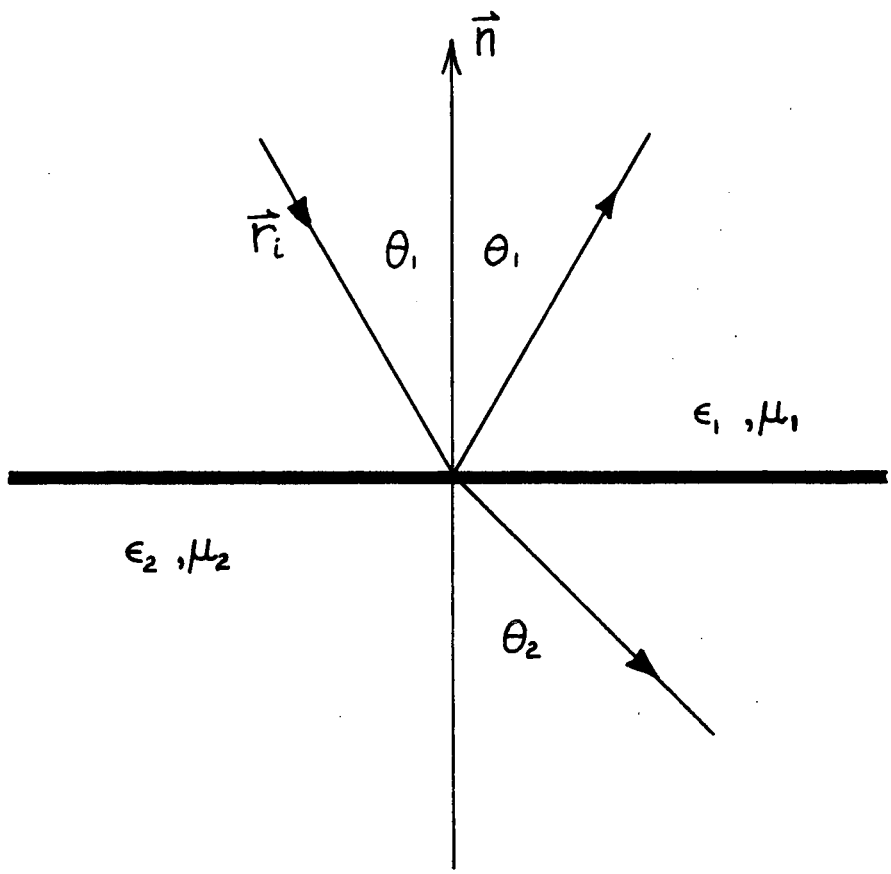

Figure IV-3

External Specular Reflection and Refraction Geometry

where n_1, n_2 are the indices of refraction ($\sqrt{\mu\varepsilon}$). The angular dependence may be written using (IV-13).

$$\frac{N^e_{\lambda V}}{I^i_{\lambda V}} = 1 - \rho_V^2 = \frac{4\eta_1\eta_2\cos\theta_1\cos\theta_2}{(\eta_1\cos\theta_1 + \eta_2\cos\theta_2)}$$

$$\frac{N^e_{\lambda H}}{I^i_{\lambda H}} = 1 - \rho_H^2 = \frac{4\eta_1\eta_2\cos\theta_1\cos\theta_2}{(\eta_1\cos\theta_2 + \eta_2\cos\theta_1)} \qquad \text{(IV-16)}$$

These equations express the angular dependence of radiation emission from a smooth surface as formulated by Peake. An alternative approach is now presented.

Planckian Method

The radiation emission from an object is considered to be that portion of the internal radiation which escapes to the surroundings. The internal spectral goniometric irradiance upon the surface is assumed to be independent of direction and randomly polarized (Lambertian), for a homogeneous isotropic material in thermodynamic equilibrium. This does not, however, imply that the radiance emitted from the upper side of the surface is Lambertian, although this is frequently assumed to be the case. The subsurface goniometric irradiance, assuming random polarization is:

$$\vec{I}_{\lambda V2} = \vec{I}_{\lambda H2} = \frac{1}{2}\vec{I}_{\lambda 2} \qquad \text{(IV-17)}$$

where $I_{\lambda 2}$ is the total spectral goniometric irradiance from medium 2 (subsurface).

Using Poyntings theorem, the subsurface goniometric irradiance may be related to the subsurface incident goniometric fields exactly as in (IV-12).

$$\vec{I}_{\lambda V2} = \vec{E}_{\lambda \Omega V} \times \vec{H}_{\lambda \Omega V}$$

$$\vec{I}_{\lambda H2} = \vec{E}_{\lambda \Omega H} \times \vec{H}_{\lambda \Omega H} \qquad \text{(IV-18)}$$

A fraction of the subsurface irradiance incident on the boundary is transmitted across and becomes the radiation emission. The emitted radiance may also be written using Poynting's theorem and the transmission characteristics of the boundary

$$\vec{N}^e_{\lambda V} = \tau_{EV2}\vec{E}_{\lambda\Omega V} \times \tau_{HV2}\vec{H}_{\lambda\Omega V}$$

$$\vec{N}^e_{\lambda H} = \tau_{EH2}\vec{E}_{\lambda\Omega H} \times \tau_{HH2}\vec{H}_{\lambda\Omega H} \qquad \text{(IV-19)}$$

where τ represents a transmission coefficient; the first subscript indicates electric (E) or magnetic (H), and the second indicates vertical (V) or horizontal (H) polarization.

Combining (IV-17), (IV-18), and (IV-19)

$$N^e_{\lambda V} = \frac{1}{2}\tau_{EV2}\tau_{HV2}I_{\lambda 2}$$

$$N^e_{\lambda H} = \frac{1}{2}\tau_{EH2}\tau_{HH2}I_{\lambda 2} \qquad \text{(IV-20)}$$

The total emitted radiance is

$$\vec{N}^e_{\lambda} = \vec{N}^e_{\lambda V} + \vec{N}^e_{\lambda H} \qquad \text{(IV-21)}$$

and the transmission coefficients are given by

$$\tau_{EV2} = \frac{2\eta_1 \cos\theta_1}{\eta_1 \cos\theta_1 + \eta_2 \cos\theta_2}$$

$$\tau_{HV2} = \frac{2\eta_2 \cos\theta_2}{\eta_1 \cos\theta_1 + \eta_2 \cos\theta_2}$$

$$\tau_{EH2} = \frac{2\eta_1 \cos\theta_2}{\eta_1 \cos\theta_2 + \eta_2 \cos\theta_1} \qquad \text{(IV-22)}$$

$$\tau_{HH2} = \frac{2\eta_2 \cos\theta_1}{\eta_1 \cos\theta_2 + \eta_2 \cos\theta_1}$$

From (IV-20) and (IV-22) it is readily seen that the angular dependence of natural radiation emission from a smooth surface is expressed. It is convenient to define a quantity which represents the ratio of emitted radiance to subsurface goniometric irradiance; the directional transmittance of the boundary is

$$\tau_{\lambda V2} = \frac{2N^e_{\lambda V}}{I_{\lambda 2}} = \frac{4\eta_1\eta_2 \cos\theta_1 \cos\theta_2}{(\eta_1 \cos\theta_1 + \eta_2 \cos\theta_2)^2}$$

$$\tau_{\lambda H2} = \frac{2N^e_{\lambda H}}{I_{\lambda 2}} = \frac{4\eta_1\eta_2 \cos\theta_1 \cos\theta_2}{(\eta_1 \cos\theta_2 + \eta_2 \cos\theta_1)^2} \qquad \text{(IV-23)}$$

It is interesting to note that this expression is exactly that as derived by Peake's method (IV-16), except that (IV-23) expresses the ratio of emission to internal thermal radiation, while (IV-16) is the ratio of emission to externally incident radiation. The difference arises from the specific assumptions of thermal equilibrium; Peake has assumed total thermal equilibirum with the surroundings, while the Planckian method involves only the assumption of internal thermal equilibrium. Obviously, the condition of internal thermal equilibirum cannot exist for long if thermal equilibirum with the surroundings is not maintained, however, it is a step in the right direction toward a general theory of thermal radiation emission.

For thermal equilibrium with the surroundings, (IV-23) reduces to (IV-16) since

$$I_{\lambda V1} = I_{\lambda V2}$$

$$I_{\lambda H1} = I_{\lambda H2}$$

The indication is that (IV-23) is a generalization of (IV-16).

The emission from a smooth surface is now obtainable. Combining (IV-1), (IV-7), and (IV-23)

$$\vec{N}^{e}_{\lambda V} = \frac{1}{2}\,\mathcal{T}_{\lambda V2}\,\epsilon_{\lambda}\,\vec{N}^{b}_{\lambda}$$

$$\vec{N}^{e}_{\lambda H} = \frac{1}{2}\,\mathcal{T}_{\lambda H2}\,\epsilon_{\lambda}\,\vec{N}^{b}_{\lambda} \qquad \text{(IV-24)}$$

The radiance of a physical object with a smooth surface is thus expressed in terms of the direction, absolute temperature of the material, and other physical parameters. This formulation also allows the use of the Rayleigh-Jean approximation when applicable ($\lambda T >> 100{,}000\mu^{o}K$).

Emission from a Rough Surface

The transmission of internal radiation to the surroundings is perturbed by the existance of irregularities at the boundary. The general problem associated with transmissive rough surface scattering is indicated in Figure IV-4, and may be treated in a manner analagous to reflective scattering (Chapter III). A quantity of electromagnetic energy, incident from the direction $\bar{r}_i$, onto an elemental area of surface dS is refracted into various directions depending on the surface roughness characteristics. As in Chapter III, it is convenient to introduce transmissive scattering coefficients defined as the ratio of the scattered electric or magnetic field into the direction $\bar{r}_s$, to the incident electric or magnetic field from the direction $\bar{r}_i$.

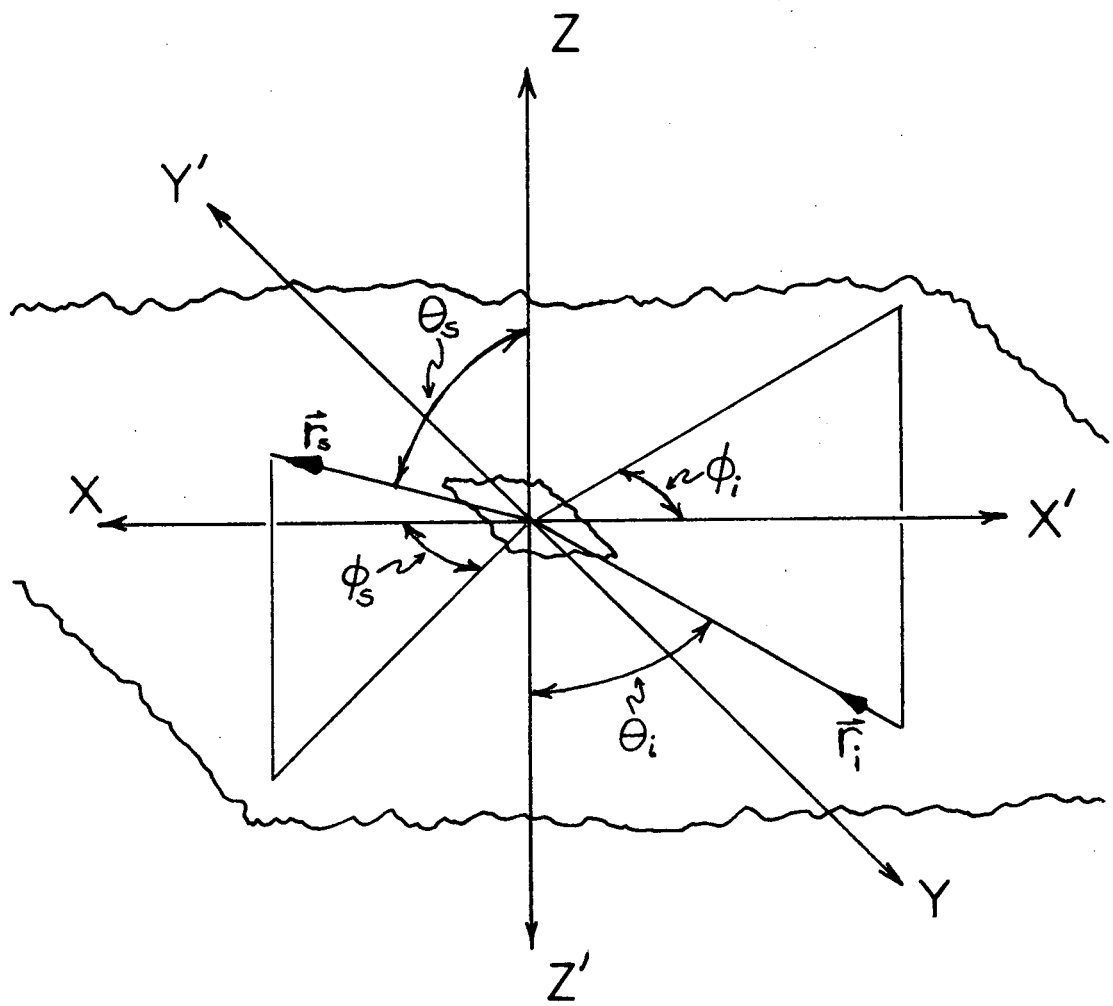

Figure IV-4

Transmissive Scattering Geometry

$$\tau_{EHH} = \frac{E_H^s}{E_H^i} \qquad \tau_{HHH} = \frac{H_H^s}{H_H^i}$$

$$\tau_{EVV} = \frac{E_V^s}{E_V^i} \qquad \tau_{HVV} = \frac{H_V^s}{H_V^i} \qquad \text{(IV-25)}$$

$$\tau_{EVH} = \frac{E_V^s}{E_H^i} \qquad \tau_{HVH} = \frac{H_V^s}{H_H^i}$$

$$\tau_{EHV} = \frac{E_H^s}{E_V^i} \qquad \tau_{HHV} = \frac{H_H^s}{H_V^i}$$

where for the field vectors, the subscripts V, H indicate vertical or horizontal polarization in relation to the mean coordinate system, and the superscripts s, i denote scattered or incident fields respectively. For the scattering coefficients, the first subscript indicates electric (E), or magnetic (H) scattering coefficient; the second indicates the polarization of the scattered field; the third indicates the polarization of the incident field.

Localized Parameters

The incident and scattered directions are indicated by their azimuth and zenith angles with respect to internal (C') and external (C) mean coordinate systems respectively as in Figure IV-4,(p. 101). The element of surface dS is presumed to contain an "effective area" oriented

such that the radiation incident from (θ_i, ϕ_i) is specularly refracted into (θ_s, ϕ_s). The "effective area" is a function of the surface roughness and of the incident and scattering directions as in Chapter III.

Local surface normals. Each incident and scattered directional pair (r_i, r_s) implies the orientation of the effective area and two local normals: external, $\bar{n}$, and internal $\bar{n}'$, which are diametrically opposed. The orientation of each is described by its zenith and azimuth angles with respect to the appropriate coordinate system (internal or external). As a result of the particular definition of the coordinate systems, the zenith and azimuth angles describing each normal are numerically equivalent and are denoted (θ_n, ϕ_n); see Figure IV-5.

Local incidence angle. The local effective normal lies in the plane formed by $\bar{r}_i$ and $\bar{r}_s$. The angle between $\bar{r}_i$ and $\bar{n}$, denoted θ_{in}, is related to the angle between $\bar{r}_s$ and $\bar{n}$, denoted θ_{sn}, by Snells' Law of refraction, and is of significance in computation of the Fresnel transmission coefficients. From Snells' Law [33]

$$n_2 \sin\theta_{in} = n_1 \sin\theta_{sn} \qquad \text{(IV-26)}$$

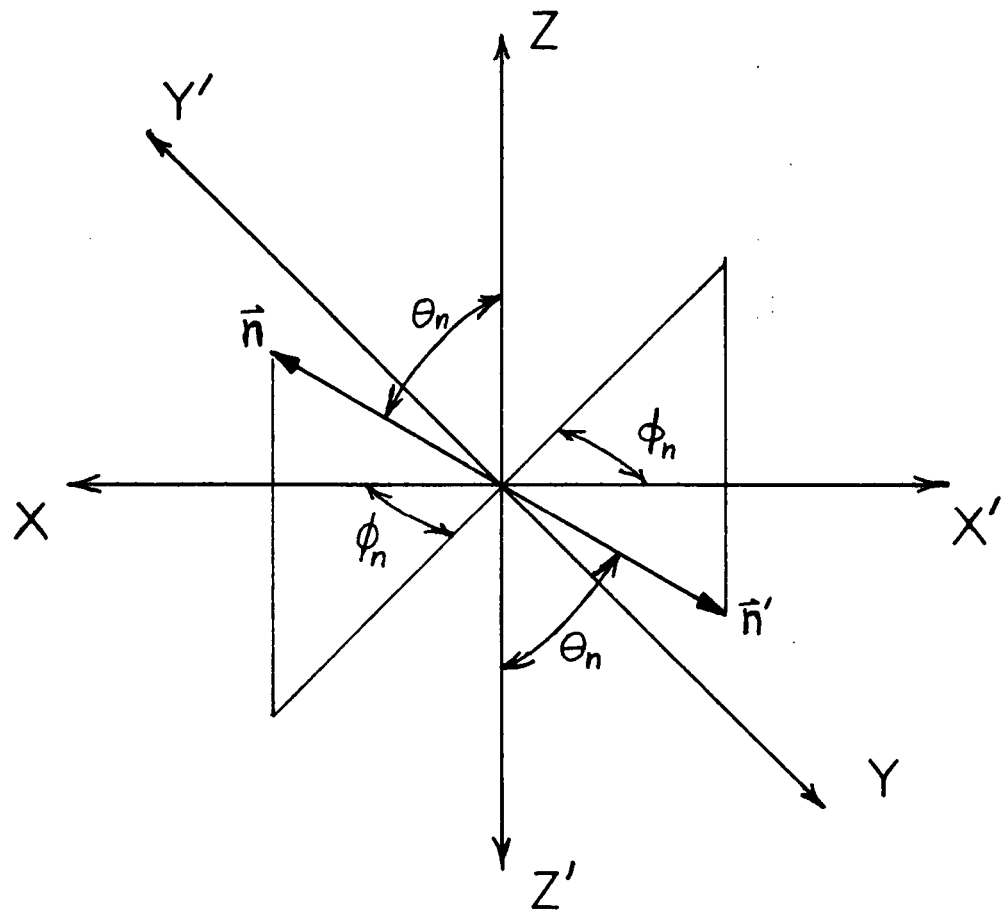

Figure IV-5

Equivalence of Local Normals

where n_1 and n_2 are the indices of refraction of upper and lower media respectively (Fig. IV-3, p. 94). The local angles of incidence (θ_{in}) and refraction (θ_{sn}) are related to the zenith and azimuth angles of $\bar{r}_i$, $\bar{r}_s$, and $\bar{n}$ by the Law of Cosines for sides of oblique spherical triangles[34] as in Chapter III;

$$\cos\theta_{in} = \cos\theta_i \cos\theta_n + \sin\theta_i \sin\theta_n \cos(\phi_n - \phi_i) \qquad \text{(IV-27)}$$

$$\cos\theta_{sn} = \cos\theta_s \cos\theta_n + \sin\theta_s \sin\theta_n \cos(\phi_n - \phi_s)$$

Local polarization. Incident radiation which is polarized vertical or horizontal in relation to the mean coordinate system appears to have vertical and horizontal components in relation to the local coordinates. By the same reasoning as in Chapter III, a simple rotation of the incident polarization coordinates about the line of incidence is sufficient to obtain a locally vertical and horizontal coordinate system. The coordinates are rotated until the vertical coordinate lies in the plane formed by $\bar{r}_i$ and $\bar{r}_s$. This angle of rotation, α_i, is obtainable using the Law of Cosines for sides of oblique spherical triangles [35];

$$\cos\alpha_i = \frac{\cos\theta_n - \cos\theta_{in}\cos\theta_i}{\sin\theta_{in}\sin\theta_i} \qquad (\text{IV-28})$$

For incident radiation consisting of vertical and horizontal polarization components, the locally polarized components are related by

$$\begin{aligned} E^i_{LV} &= E^i_V \cos\alpha_i + E^i_H \sin\alpha_i \\ E^i_{LH} &= E^i_H \cos\alpha_i - E^i_V \sin\alpha_i \\ H^i_{LV} &= H^i_V \cos\alpha_i + H^i_H \sin\alpha_i \\ H^i_{LH} &= H^i_H \cos\alpha_i - H^i_V \sin\alpha_i \end{aligned} \qquad (\text{IV-29})$$

Here, the subscripts LV and LH indicate locally vertical and horizontal components respectively. The local scattered components into the direction $\bar{r}_s$ is

$$\begin{aligned} E^s_{LV} &= \tau_{EV} E^i_{LV} \\ E^s_{LH} &= \tau_{EH} E^i_{LH} \end{aligned} \qquad (\text{IV-30})$$

$$H^s_{LV} = \tau_{HV} H^i_{LV}$$

$$H^s_{LH} = \tau_{HH} H^i_{LH}$$

where the Fresnel transmission coefficients are given by (IV-22), and for this geometry

$$\theta_1 = \theta_{sn}$$

$$\theta_2 = \theta_{in} \qquad \text{(IV-31)}$$

The local scattered components are related to mean scattered components by a rotation α_r of polarization coordinates about the line of propagation. By the same method as α_i was obtained,

$$\cos \alpha_r = \frac{\cos \theta_n - \cos \theta_{sn} \cos \theta_s}{\sin \theta_{sn} \sin \theta_s} \qquad \text{(IV-32)}$$

The mean scattered fields are

$$E_V^s = E_{LV}^s \cos\alpha_r - E_{LH}^s \sin\alpha_r$$

$$E_H^s = E_{LH}^s \cos\alpha_r + E_{LV}^s \sin\alpha_r$$

$$H_V^s = H_{LV}^s \cos\alpha_r - H_{LH}^s \sin\alpha_r \qquad \text{(IV-33)}$$

$$H_H^s = H_{LH}^s \cos\alpha_r + H_{LV}^s \sin\alpha_r$$

Combining (IV-29), (IV-30) and (IV-33)

$$E_V^s = \tau_{EV}\left[E_V^i \cos\alpha_i + E_H^i \sin\alpha_i\right]\cos\alpha_r - \tau_{EH}\left[E_H^i \cos\alpha_i - E_V^i \sin\alpha_i\right]\sin\alpha_r$$

$$E_H^s = \tau_{EH}\left[E_H^i \cos\alpha_i - E_V^i \sin\alpha_i\right]\cos\alpha_r + \tau_{EV}\left[E_V^i \cos\alpha_i + E_H^i \sin\alpha_i\right]\sin\alpha_r \qquad \text{(IV-34)}$$

$$H_V^s = \tau_{HV}\left[H_V^i \cos\alpha_i + H_H^i \sin\alpha_i\right]\cos\alpha_r - \tau_{HH}\left[H_H^i \cos\alpha_i - H_V^i \sin\alpha_i\right]\sin\alpha_r$$

$$H_H^s = \tau_{HH}\left[H_H^i \cos\alpha_i - H_V^i \sin\alpha_i\right]\cos\alpha_r + \tau_{HV}\left[H_V^i \cos\alpha_i + H_H^i \sin\alpha_i\right]\sin\alpha_r$$

where the Fresnel transmission coefficients are given by (IV-22) in conjunction with (IV-8) and (IV-31).

Scattering coefficients. The transmissive scattering coefficients as defined by (IV-25) are obtainable from (IV-34)

$$\tau_{EHH} = \tau_{EH} \cos\alpha_i \cos\alpha_r + \tau_{EV} \sin\alpha_i \sin\alpha_r$$

$$\tau_{EVV} = \tau_{EV} \cos\alpha_i \cos\alpha_r + \tau_{EH} \sin\alpha_i \sin\alpha_r$$

$$\tau_{EVH} = \tau_{EV} \sin\alpha_i \cos\alpha_r - \tau_{EH} \cos\alpha_i \sin\alpha_r$$

$$\tau_{EHV} = \tau_{EV} \cos\alpha_i \sin\alpha_r - \tau_{EH} \sin\alpha_i \cos\alpha_r \qquad \text{(IV-35)}$$

$$\tau_{HHH} = \tau_{HH} \cos\alpha_i \cos\alpha_r + \tau_{HV} \sin\alpha_i \sin\alpha_r$$

$$\tau_{HVV} = \tau_{HV} \cos\alpha_i \cos\alpha_r + \tau_{HH} \sin\alpha_i \sin\alpha_r$$

$$\tau_{HVH} = \tau_{HV} \sin\alpha_i \cos\alpha_r - \tau_{HH} \cos\alpha_i \sin\alpha_r$$

$$\tau_{HHV} = \tau_{HV} \cos\alpha_i \sin\alpha_r - \tau_{HH} \sin\alpha_i \cos\alpha_r$$

where τ_{EV}, τ_{EH}, τ_{HV}, τ_{HH} are the Fresnel reflection coefficients given by (IV-22) and (IV-31); α_i, α_r, are the incident and scattered rotations of polarization coordinates into the local plane of incidence given by (IV-28) and (IV-32). Also, if the incident and refracted directions are interchanged, the theorem of reciprocity is not violated by this formulation. These coefficients represent the transmission characteristics of plane elemental surfaces as a function of their orientation with respect to the mean coordinate system; they do not account for the relative quantities of effective area available for specular refraction from each incident and scattered directional pair (r_i, r_s).

Surface Model

The surface model presented in the previous chapter is applicable to the present problem; the effective area and actual area per unit mean surface are given in terms of the statistical properties of the surface roughness. The results are given again here for convenience

$$\delta = \frac{dS}{dA} = \frac{1}{\int_0^{\pi/2} f_\theta(\theta_n) \cos\theta_n \, d\theta_n} \qquad \text{(IV-36)}$$

$$\beta = \frac{dA_{eff}}{dS} = \frac{f_\theta(\theta_n)}{2\pi \sin\theta_n} \qquad (IV-37)$$

where: $f_\theta(\theta)$ = probability density function for the zenith angle of the surface normal

Phase Interference

As indicated in Appendix B, under the assumption of random incident phase, there are no average phase interference effects in the scattered field from the elementary area of surface.

Power Scattering Coefficients

The power scattering coefficients are now obtainable. The incident goniometric polarized irradiance may be written using Poynting's theorem, [36]

$$\vec{I}_{\lambda V} = \vec{E}^i_V \times \vec{H}^i_V$$

$$\vec{I}_{\lambda H} = \vec{E}^i_H \times \vec{H}^i_H \qquad (IV-38)$$

where: $(I_{\lambda V}, I_{\lambda H})$ = (vertical, horizontal) components of the incident goniometric irradiance

$E^i_V, E^i_H, H^i_V, H^i_H$ = incident electric magnetic fields from the direction (θ_i, ϕ_i)

Of this irradiance, a certain fraction falls on the effective area and is subsequently available for specular refraction into the direction (θ_s, ϕ_s). The fraction was given in Chapter III and is

$$I_{\lambda V}^{eff} = \frac{\cos\theta_i}{\beta\delta\cos\theta_{in}} I_{\lambda V}$$

$$I_{\lambda H}^{eff} = \frac{\cos\theta_i}{\beta\delta\cos\theta_{in}} I_{\lambda V} \qquad \text{(IV-39)}$$

representing the irradiance from (θ_i, ϕ_i) which falls on effective area. The effective scattered polarized radiance is

$$\vec{N}_{\lambda V} = \vec{E}_V^S \times \vec{H}_V^S$$

$$\vec{N}_{\lambda H} = \vec{E}_H^S \times \vec{H}_H^S \qquad \text{(IV-40)}$$

where: $N_{\lambda V}$, $N_{\lambda H}$ = vertical, horizontal components of scattered radiance

E_V^S, E_H^S, H_V^S, H_H^S = effective scattered fields

The effective incident and refracted fields per unit solid angle per unit effective area are related by the scattering coefficients (IV-35), therefore the scattered

polarized radiance becomes

$$\vec{N}_{\lambda V} = \left(\tau_{EVV}\vec{E}^{i}_{V} + \tau_{EVH}\vec{E}^{i}_{H}\right) \times \left(\tau_{HVV}\vec{H}^{i}_{V} + \tau_{HVH}\vec{H}^{i}_{H}\right) \tag{IV-41}$$

$$\vec{N}_{\lambda H} = \left(\tau_{EHH}\vec{E}^{i}_{H} + \tau_{EHV}\vec{E}^{i}_{V}\right) \times \left(\tau_{HHH}\vec{H}^{i}_{H} + \tau_{HHV}\vec{H}^{i}_{V}\right)$$

Expanding the cross products and realizing

$$\vec{E}^{i}_{V} \times \vec{H}^{i}_{H} = \vec{E}^{i}_{H} \times \vec{H}^{i}_{V} = \vec{O}$$

gives

$$\vec{N}_{\lambda V} = \tau_{EVV}\,\tau_{HVV}\left(\vec{E}^{i}_{V} \times \vec{H}^{i}_{V}\right) + \tau_{EVH}\,\tau_{HVH}\left(\vec{E}^{i}_{H} \times \vec{H}^{i}_{H}\right) \tag{IV-42}$$

$$\vec{N}_{\lambda H} = \tau_{EHH}\,\tau_{HHH}\left(\vec{E}^{i}_{H} \times \vec{H}^{i}_{H}\right) + \tau_{EHV}\,\tau_{HHV}\left(\vec{E}^{i}_{V} \times \vec{H}^{i}_{V}\right)$$

where the cross products represent the effective irradiance and are given by (IV-39). Substituting (IV-39) into (IV-42),

$$N_{\lambda V} = \frac{\cos\theta_i}{\beta\delta\cos\theta_{in}}\left[\tau_{EVV}\,\tau_{HVV}\,I_{\lambda V} + \tau_{EVH}\,\tau_{HVH}\,I_{\lambda H}\right] \tag{IV-43}$$

$$N_{\lambda H} = \frac{\cos\theta_i}{\beta\delta\cos\theta_{in}}\left[\tau_{EHH}\,\tau_{HHH}\,I_{\lambda H} + \tau_{EHV}\,\tau_{HHV}\,I_{\lambda V}\right]$$

where $\beta\delta$ is expressed by (IV-36) and (IV-32) and the scattering coefficients are given by (IV-35).

For the smooth surface case

$$\beta = \delta = 1 , \cos\theta_{in} = \cos\theta_i$$

$$\tau_{EVV} = \tau_{EV} \quad , \quad \tau_{HVV} = \tau_{HV}$$

$$\tau_{EHH} = \tau_{EH} \quad , \quad \tau_{HHH} = \tau_{HH}$$

$$\tau_{EVH} = \tau_{EHV} = \tau_{HVH} = \tau_{HHV} = 0$$

Therefore equation (IV-43) becomes for a smooth surface

$$N_{\lambda V} = \tau_{EV}\,\tau_{HV}\,I_{\lambda V}$$

$$N_{\lambda H} = \tau_{EH}\,\tau_{HH}\,I_{\lambda H} \qquad \text{(IV-44)}$$

which is the result to be expected.

CHAPTER V

CONCLUSIONS AND RECOMMENDATIONS

The interpretation of remotely sensed infrared data is inhibited by an inability to account for the radiative characteristics of targets. Existing performance figures for infrared systems viewing extended targets exhibit the dependence of system performance on target radiance characteristics, but current theories fail to completely predict the nature of thermal emission and background reflection from targets.

The theory presented in Chapter III provides the basis for an analytical model of rough surface reflective scattering characteristics. The resulting expressions for the polarized reflection may be written as functions of material properties, surface statistics, and incident and viewing directional angles only. Two equations result (one for each polarization, vertical or horizontal) which describe the radiance into any direction due to the reflection of the goniometric irradiance on a small area of surface from a single direction. The total radiance due to reflection of all incident radiation may be obtained through integration of each polarized radiance expression over all incident directions. The indicated integration appears at best to be very difficult, since the argument is an ex-

tremely complex ratio of trigonometric expressions.

Analagous expressions describing the thermal radiation emission from extended targets are formulated in Chapter IV. Again, expressions in terms of material properties, surface statistics, and incident and viewing directions only, may be obtained although their complexity severely limits their utility. Integration over the incident directions results in two expressions (one for each polarization) for the thermally emitted radiance.

The total radiative characteristics of the target are expressed by these results. The radiance in any direction is the sum of the reflected radiance (Chapter III) and the emitted radiance (Chapter IV), although several assumptions and limitations must be noted.

The results indicate a degree of correctness as illustrated in the concluding pages of Chapter III and Chapter IV, where the expressions exhibit reduction to known results for the special case of a smooth surface. This reduction, in itself, warrants further investigation into the possible simplification of the resulting formulation.

In the formulation of the thermal radiation generation it was assumed the material was homogeneous, isotropic, and in a state of thermal equilibrium, assumptions which are not always valid for the general case. Further study is required to determine the nature of internal radiation in

the absence of these assumptions. The directional transmission characteristics of the surface are unaffected by these assumptions and hence are valid (within limitations) for use with any formulation of internal goniometric irradiance on the surface.

The limitations on the validity of the reflective and transmissive scattering theory arise from failure to consider certain phenomena which are known to occur during scattering from rough surfaces. The local radii of curvature have a dispersive effect on scattered radiation; also, multiple scattering and shadowing effects modify the reflection and transmission characteristics of the surface. It is believed that the theory can be extended to include these effects.

In remote sensing studies employing infrared measurements, especially images, the relationship between recorded data and the environmental situation is often assumed to be a simple one. The radiative characteristics of the target and the performance of the sensor are frequently ignored. This thesis establishes that, in fact, the relationship is quite complex involving characteristics of the sensor in addition to properties of the target. Hence considerably more attention must be given to the effects of material composition and surface roughness characteristics in order to accurately interpret remote sensing data.

REFERENCES

[1] D. C. Parker, M. F. Wolff, "Remote Sensing," International Science and Technology, July 1965.

[2] G. A. Rabchevsky, "Remote Sensing of the Earth's Surface," in 3 parts, Journal of Remote Sensing, June-July 1970, p. 15, August-September 1970, p. 5, November-December 1970, p. 14.

[3] _____, Proceedings of the First Symposium on Remote Sensing of Environment, University of Michigan, Ann Arbor, February 1962.

[4] _____, Proceedings of the Second Symposium on Remote Sensing of Environment, University of Michigan, Ann Arbor, October 1962.

[5] _____, Proceedings of the Third Symposium on Remote Sensing of Environment, University of Michigan, Ann Arbor, October 1964.

[6] _____, Proceedings of the Fourth Symposium on Remote Sensing of Environment, University of Michigan, Ann Arbor, April 1966.

[7] _____, Proceedings of the Fifth Symposium on Remote Sensing of Environment, University of Michigan, Ann Arbor, April 1968.

[8] _____, Proceedings of the Sixth Symposium on Remote Sensing of Environment, University of Michigan, Ann Arbor, October 1969.

[9] _____, Proceedings of the Seventh Symposium on Remote Sensing of Environment, University of Michigan, Ann Arbor, May 1971.

[10] R. D. Hudson Jr., Infrared System Engineering. New York: John Wiley and Sons, 1969.

[11] E. G. Wermund, "Remote Sensors for Hydrogeologic Prospecting in Arid Terrains," IEEE Transactions on Geoscience Electronics, vol. GE-9, July 1971, p. 120.

[12] N. G. Foster, "Aerial 8-14 Micron Imagery Applied to Mapping Thermal Effect Mixing Boundaries," Masters Thesis, Interdisciplinary Engineering, Texas A&M University, College Station, Texas, August 1970.

[13] R. D. Hudson Jr., Infrared System Engineering. New York: John Wiley and Sons, 1969, pp. 216-218.

[14] op. cit., pp. 195-206.

[15] R. C. Jones, "Phenomenological Description of the Response and Detecting Ability of Radiation Detectors," Proceedings IRE, vol. 47, September 1959, p. 1495.

[16] R. D. Hudson Jr., Infrared System Engineering. New York: John Wiley and Sons, 1969, p. 294.

[17] op. cit., p. 272.

[18] op. cit., p. 419.

[19] R. H. Genoud, "Infrared Search System Range Performance," Proceedings IRE, vol. 47, September 1959, pp. 1581-1586.

[20] R. D. Hudson Jr., Infrared System Engineering. New York: John Wiley and Sons, 1969, p. 431.

[21] C. A. Klein, "Thermal Imaging Performance of Passive Infrared Scanners," IEEE Transactions on Geoscience Electronics, vol. GE-9, July 1971, pp. 139-146.

[22] W. H. Peake, D. E. Barrick, "Scattering from Surfaces With Different Roughness Scales: Analysis and Interpretation," Research Report No. BAT-197A-10-3 Battele Memorial Institute, Columbus Laboratories, Columbus, Ohio, 1967.

[23] _____, CRC Standard Math Tables, 15th Student Edition, The Chemical Rubber Company, Cleveland, Ohio, 1967, p. 162.

[24] op. cit., p. 162.

[25] S. Ramo, J. R. Whinnery, T. Van Duzer, Fields and Waves in Communication Electronics. New York: John Wiley and Sons, 1965, p. 360.

[26] op. cit., p. 360.

[27] A. Papoulis, Probability, Random Variables, and Stochastic Processes. New York: McGraw Hill Book Company, 1965, p. 94.

[28] M. Planck, The Theory of Heat Radiation, New York: Dover Publications, Inc., 1959.

[29] op. cit., p. 21.

[30] W. H. Peake, "Interaction of Electromagnetic Waves with Some Natural Surfaces," IRE Transactions on Antennas and Propagation, December 1959, p. 324.

[31] S. Ramo, J. R. Whinnery, T. Van Duzer, Fields and Waves in Communication Electronics. New York: John Wiley and Sons, Inc., 1965, p. 360.

[32] op. cit., p. 360.

[33] op. cit., p. 359.

[34] _____, CRC Standard Math Tables, 15th Student Edition, The Chemical Rubber Company, Cleveland, Ohio, 1967, p. 162.

[35] op. cit., p. 162.

[36] S. Ramo, J. R. Whinnery, T. Van Duzer, Fields and Waves in Communication Electronics. New York: John Wiley and Sons, Inc., 1965, p. 242.

[37] G. Kelton, et. al., "Infrared Target and Background Radiometric Measurements - Concepts, Units and Techniques," Infrared Physics, vol. 3, 1963, p. 139.

[38] I. Simon, Infrared Radiation. Princeton, New Jersey: D. Van Nostrand and Company, Inc. 1966, p. 14.

APPENDIX A

RADIATION CONCEPTS

The purpose of this appendix is to provide a firm basis for the theory and terminology presented in the main body of this thesis. Radiometric quantities, symbols, and units have a tendency to be rather cumbersome, and consequent improper usage is frequent. Successful communication among researchers can be accomplished only if a concentrated effort is made toward the use of precise terminology.

Terminology

The large number of terms available to differentiate among radiation as a function of various parameters, (angle, surface area, wavelength) is generally responsible for the resulting misuse. Also, several different sets of terms have been developed to describe the various quantities of radiometric interest. To aid proper interpretation of this thesis, the pertinent symbols, terms, and definitions are included in Table A-1. As much as possible, the symbols and definitions conform to the recommendations of the Working Group on Infrared Backgrounds (WGIRB) [37] and are consistent with American Standard Z58.1.1-1953.

Several of these terms and symbols require further

TABLE A-1

RADIOMETRIC TERMINOLOGY

Symbol	Term	Description
U	Radiant Energy	Energy transferred by EM waves
u	Radiant Energy Density	Radiant energy per unit volume
P	Radiant Power	Rate of radiant energy transfer
W	Radiant Emittance	Radiant power emitted per unit area
J	Radiant Intensity	Radiant power per unit solid angle
N	Radiance	Radiant power per unit solid angle per unit area
H	Irradiance	Incident radiant power per unit area
I	Goniometric Irradiance	Incident radiant power per unit solid angle per unit area
ε'	emissivity	Ratio of internal radiant energy density of a material to that of a blackbody
ε	emissance	Ratio of radiant emittance of a source to that of a blackbody
subscripts		
λ, ν	spectral _____	per unit (wavelength, frequency) interval
superscript		
b	blackbody _____	pertaining to a blackbody source

discussion. Special attention should be given to the term goniometric irradiance, designated by the symbol, I, which refers to incident radiation power per unit solid angle per unit surface area. This term is not generally included in tables of radiometric terminology but is useful in the development presented in Chapter IV.

Another clarification is required, regarding all radiometric quantities defined per unit area (radiant emittance, irradiance, radiance, goniometric irradiance) since various definitions of unit area are possible. Frequently, for the case of radiance or goniometric irradiance, the unit area is defined as a unit projection of the actual surface area into the viewing direction. This definition is useful as it provides a convenient reference area for rough surfaces. Blackbody radiance defined in this manner varies as the cosine of the zenith angle, obeying Lambert's cosine law, and is, hence, termed Lambertian radiance. The unit area may also be defined as a unit area of actual surface or, as in the case of radiant emittance or irradiance, a unit area on the mean surface plane. For the sake of simplicity, any reference in this thesis to radiant emittance or irradiance implies a unit mean surface area and any reference to radiance or goniometric irradiance implies a unit projected area, unless otherwise stated.

The subscripts λ and ν indicate quantities per unit

wavelength or frequency interval. The superscript, b, indicates blackbody radiation quantities. The symbol ε is normally used to denote emissivity, a term which is frequently misused. Emissivity indicates an intrinsic property of a type of material and must be differentiated from emissance which includes the effect of the surface characteristics of a particular sample of the material. In this thesis, the greek letter, ε, is used to denote emissance and ε' is used to denote emissivity.

Blackbody Radiation

Radiation theory is based on theoretical objects, blackbodies, which exhibit perfect emission and absorption characteristics. Although naturally occurring materials may approach blackbody radiation characteristics, true blackbodies do not exist. It is possible, however, to relate the radiation characteristics of natural materials to theoretical blackbody radiation laws.

Planck's Law

The radiation from a blackbody has been formulated by Planck on the basis of quantum energy level considerations, and may be expressed as a function of wavelength or frequency of the emitted radiation. The wavelength expression for blackbody spectral radiant emittance is

$$W_\lambda^b = C_1 \lambda^{-5} \left[EXP\left(\frac{C_2}{\lambda T}\right) - 1 \right]^{-1} \quad (A-1)$$

where: $c_1 = 2\pi hc^2 = 3.7415 \times 10^4$ watt$\cdot\mu^4/cm^2$

$c_2 = hc/k = 1.43879 \times 10^4 \mu \cdot °K$

h = Planck's constant = $(6.6256 \times 10^{-34} W \cdot sec^2)$

c = speed of light = $(2.997925 \times 10^{10}$ cm/sec)

k = Boltzmann's constant = $(1.38054 \times 10^{-23} W \cdot sec/°K)$

λ = wavelength

T = absolute temperature

A graphical representation of blackbody spectral radiant emittance (per unit wavelength, λ) for various temperatures is shown in Figure A-1. The spectral radiant emittance (per unit frequency, ν) is related to the spectral radiant emittance (per unit wavelength) by

$$W_\lambda^b \, d\lambda = W_\nu^b \, d\nu \quad (A-2)$$

and

$$d\lambda = \lambda^2 c \, d\nu \quad (A-3)$$

Combining (A-2) and (A-3)

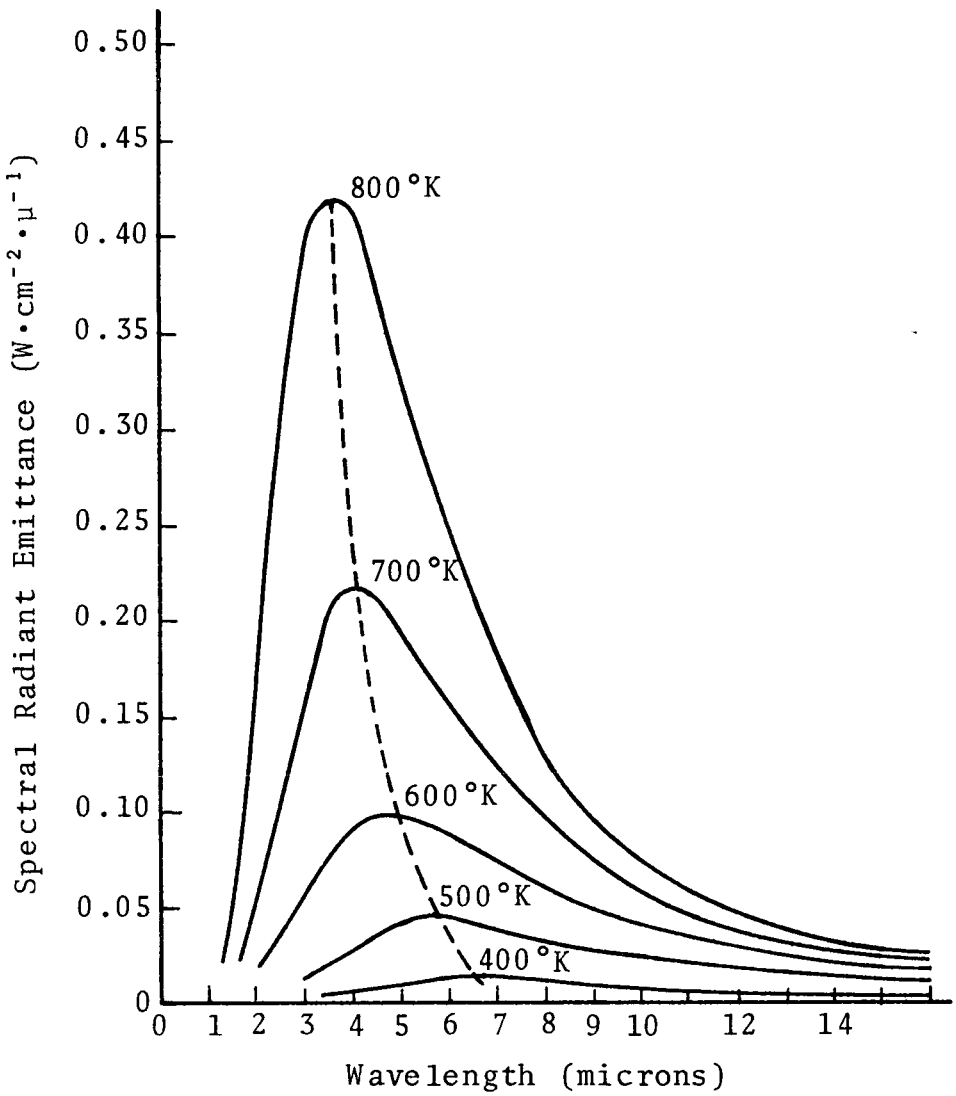

FIGURE A-1. Blackbody Radiation Curves

$$W_\nu^b = W_\lambda^b \lambda^2 C$$

or

$$W_\nu^b = C_1 \frac{\nu^3}{C^2} \left[EXP\left(\frac{C_2 \nu}{C T}\right) - 1 \right]^{-1} \quad (A-4)$$

Rayleigh-Jean's Law

An approximate expression for blackbody spectral radiant emittance is provided by Rayleigh-Jean's Law, which although formulated empirically before Planck's Law, was later found to be a special case. Expanding the exponential term of (A-1) in a power series provides the basis for obtaining Rayleigh-Jean's Law from Planck's Law. Under certain conditions ($\lambda T >> 100{,}000 \mu°K$) [38] the second and higher order terms of the expansion may be neglected, resulting in Rayleigh-Jean's approximation:

$$W_\lambda^b \simeq \frac{C_1}{C_2} T \lambda^{-4} \quad (A-5)$$

This expression offers a good approximation at very high temperatures or at very long wavelengths but obviously can not be correct at short wavelengths, since it predicts infinite power as λ approaches zero.

Wien's Displacement Law

A maximum in the blackbody spectral radiant emittance curves occurs at progressively shorter wavelengths for increasing temperature, as indicated by the dashed line in Figure A-1 (p. 126). Differentiating (A-1) with respect to wavelength, the maximum spectral radiant emittance (per unit wavelength) occurs at

$$\lambda^{b}_{max} = \frac{C_3}{T} \qquad (A-6)$$

where: $C_3 = 2897.8\mu°K$

The value of the maximum spectral radiant emittance is obtained by substituting the wavelength of the maximum, (A-5), into (A-1)

$$W^{b}_{\lambda_{max}} = C_4 T^5 \qquad (A-7)$$

where: $C_4 = 1.2862 \times 10^{-15}$ watt/cm$^2 \cdot \mu \cdot °K$

Stefan-Boltzmann's Law

An expression for the total radiant emittance from a blackbody is obtained by integrating (A-1) over all wavelengths or (A-4) over all frequencies. Thus,

$$W^b = \int_0^\infty W_\lambda^b \, d\lambda = \int_0^\infty W_\nu^b \, d\nu = \sigma T^4 \qquad (A-8)$$

where: σ = Stefan-Boltzmann constant

$= 5.6697 \times 10^{-12}$ watt/cm$^2 \cdot$°K^4

Blackbody Radiance

The radiance from a blackbody is independent of direction: a consequence of its Lambertian nature and of the particular selection of unit area in the definition. It is related to the radiant emittance by

$$W^b = N^b \pi \qquad (A-9)$$

(Note that the relationship is not $W = N2\pi$ as might be reasoned from the fact that there are 2π steradians in a hemisphere.) Equation (A-9) was obtained by integrating the radiance over the hemisphere

$$W = \int_{2\pi} N \, d\Omega \qquad (A-10)$$

while paying special attention to the different definitions of unit area for radiance and radiant emittance.

Non-blackbody Radiation

The radiation from natural objects does not obey blackbody radiation laws. It is dependent upon such parameters as temperature, surface roughness, wavelength, or material properties. But radiation from natural objects cannot exceed blackbody radiation for any temperature and wavelength. Most materials that are electrical insulators obey Lambert's Law for zenith angles below about 60°, while materials that are electrical conductors approximate Lambertian radiance within engineering accuracy for zenith angles less than about 50°.

To account for their imperfect nature, natural materials are said to have an associated emissivity which expresses the degree to which a material approximates a blackbody. It is commonly defined as the ratio of the material's radiant emittance to that of a blackbody. The suffix "ivity", however, indicates an intrinsic property of a material, which is not compatable with the previous definition since that ratio includes surface effects. Therefore, for the purpose of this thesis, the term *emissance*, ε, is used to indicate the ratio of a material's radiant emittance to that of a blackbody,

$$\epsilon = \frac{W}{W^b}$$

and the term *emissivity*, ε', is used to indicate the ratio of the internal volume density of radiation of a material to that of a blackbody. Thus, emissance includes the effect of the emissivity of a material in addition to the influence of surface characteristics.

Several problems are still inherent in this approach. In general, the emissance is known to vary with wavelength and surface roughness. Also, typical measurements are of spectral radiance, not radiant emittance, since it is difficult to measure total radiation over all frequencies and directions. For convenience, a spectral goniometric (directional) emissance is defined:

$$\epsilon_\lambda(\theta,\phi) = \frac{N_\lambda(\theta,\phi)}{N_\lambda^b} \qquad (A-11)$$

Angular and spectral dependencies are not known in general, although for certain applications, they may be averaged and assumed constant over appropriate angular and spectral intervals. Also, emissance is an empirical quantity, which is difficult to measure accurately. In Chapter IV a theoretical approach is presented, which clarifies the non-blackbody radiation problem through a new approach. Spectral goniometric emissance is theoretically derived in terms of other physical quantities, including emissivity, thus displaying an increased relationship of radiometric data to the physical situation.

APPENDIX B

PHASE INTERFERENCE OF SCATTERED RADIATION

Electromagnetic radiation incident upon rough surfaces is scattered into both media by reflection and refraction. Assuming that the incident radiation arrives in phase, the distribution of surface heights introduces phase modulation of the scattered radiation. Consequently, the scattered radiation pattern exhibits a definite lobe structure due to the phase relationships among the scattered components. Examination of this phenomena requires the introduction of a joint probability density of surface heights and directions of the local normal $f_{\theta\phi z}(\theta_n, \phi_n, z)$ which describes the vertical distribution of each effective area.

Path Length

The path difference for radiation reflected from effective areas at different heights above the mean surface is a straight forward geometrical problem. Figure B-1 depicts two incident rays, one reflected from an element of effective area at height z' and the other at the mean plane. The path difference is

$$\ell_z = Z'(\cos\theta_i + \cos\theta_s) \qquad (B\text{-}1)$$

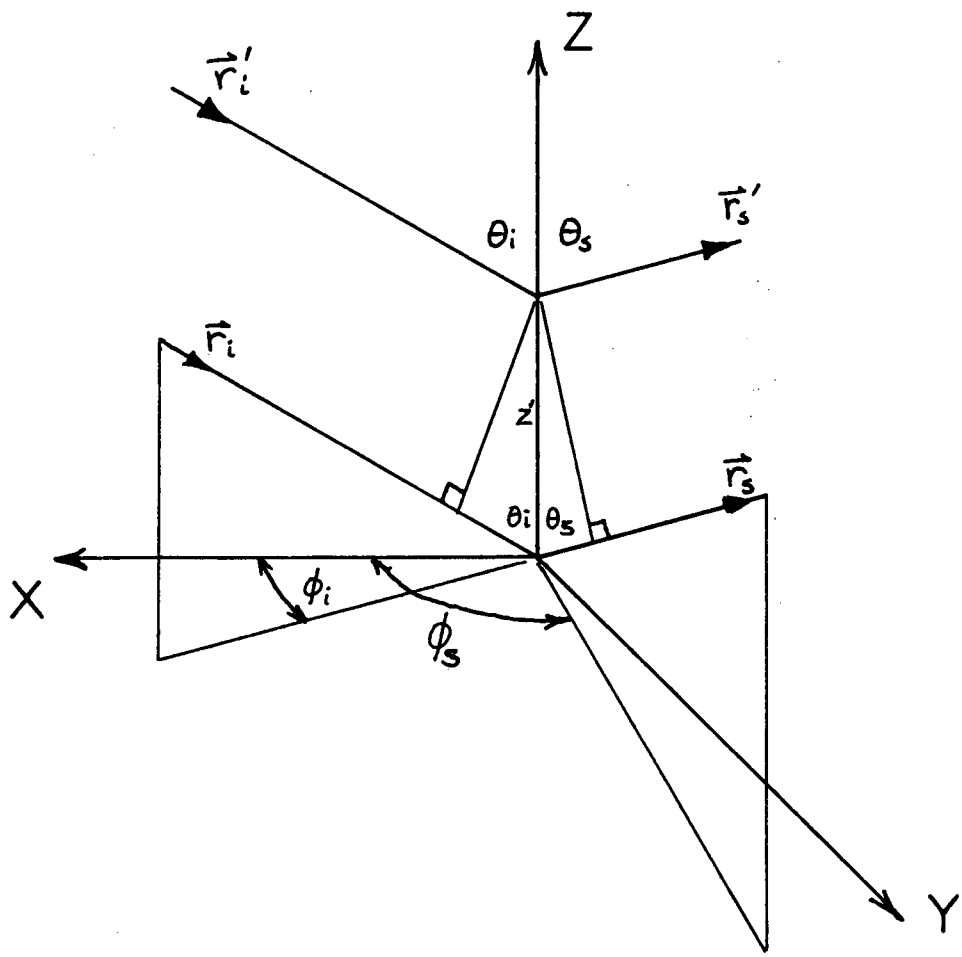

Figure B-1

Relationship of Path Lengths Due to Different Surface Heights

The element of effective area at each height is now assumed to be uniformly distributed over the mean area element, dA. The path difference for radiation reflected from different elements of effective area at the same height above the mean plane is found as follows. Figure B-2 shows two incident rays; one is reflected from an effective area at the origin of the mean coordinate system and the other is reflected from an effective area located a distance, d, away, also on the mean plane. The path difference is given by

$$\ell_d = d\left(\cos\alpha_1 + \cos\alpha_2\right) \qquad (B-2)$$

where d is the separation of the two elemental areas and

$$\cos\alpha_1 = \sin\theta_i \cos\left(\phi_d - \phi_i\right) \qquad (B-3)$$

$$\cos\alpha_2 = \sin\theta_s \cos\left(\phi_s - \phi_d\right)$$

where ϕ_d is the angle of orientation of d with respect to the x-axis of the mean coordinate plane. The coordinate pair (d, ϕ_d) represent a polar coordinate system in the x-y plane. The uniform distribution of effective area over dA is accomplished by assigning a uniform distribution

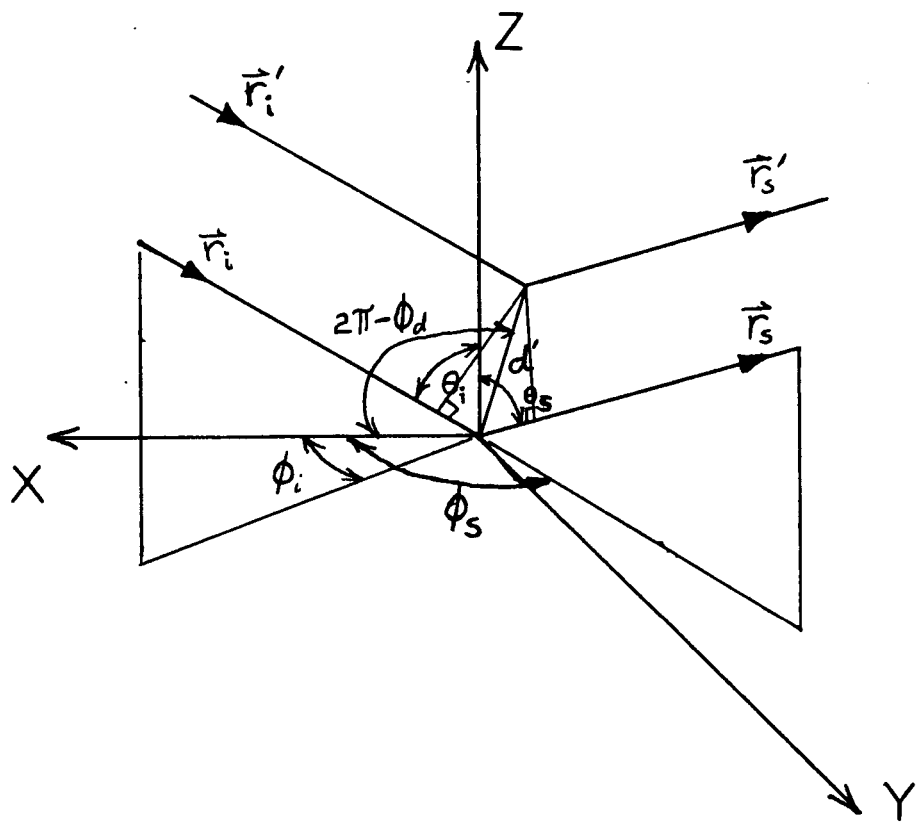

Figure B-2

Relationship of Path Lengths Due to Different Surface Locations

to the polar coordinates (d, ϕ_d).

Phase Difference

The total path length difference due to surface height and position variations is given by

$$\ell = \ell_z + \ell_d \qquad (B-4)$$

which corresponds to a phase difference of

$$\Phi = \frac{2\pi}{\lambda} \ell \qquad (B-5)$$

It is apparent for this formulation that if the surface height variation is small ($<<\lambda$), the phase interaction becomes negligible, although the surface roughness continues to be a factor in the directional reflectance and transmittance characteristics.

Random Incident Phase

The particular case of random incident phase is of special interest in the examination of thermal emission and background reflection. Given a number of periodic monochromatic waveforms, each with a specific phase with

respect to a reference, random phase does not mean that instantaneously there is an equal number of waveforms of each phase. It means that the probability of any particular phase is precisely equal to the probability of any other phase but in the instantaneous case there must be a certain distribution of phases (Figure B-3). The instantaneous phase distribution of incident radiation may be combined with the distributions for d, z, and ϕ_d and (B-5) to find the instantaneous phase distribution of scattered radiation which in general, has some definable form different from the incident instantaneous phase distribution.

Consider a single incident phase component, Φ_1', represented by a phasor in Figure B-4; the phase distribution after reflection is of some definite form which is relatable to the incident phase and the surface characteristics (Figure B-4a). This relationship cannot favor any particular phase, therefore, a second incident phase component Φ_2'' rotated in phase by $\Delta\Phi'$ from Φ_1' (Figure B-4b), produces a scattered phase distribution which is given by a simple rotation by $\Delta\Phi'$ of all components of the scattered phase distribution of Φ_1', (Figure B-4b).

Now consider an incident distribution of phases as in Figure B-5a; the scattered phase distribution is represented in Figure B-5b. A phase rotation $\Delta\Phi'$ of the

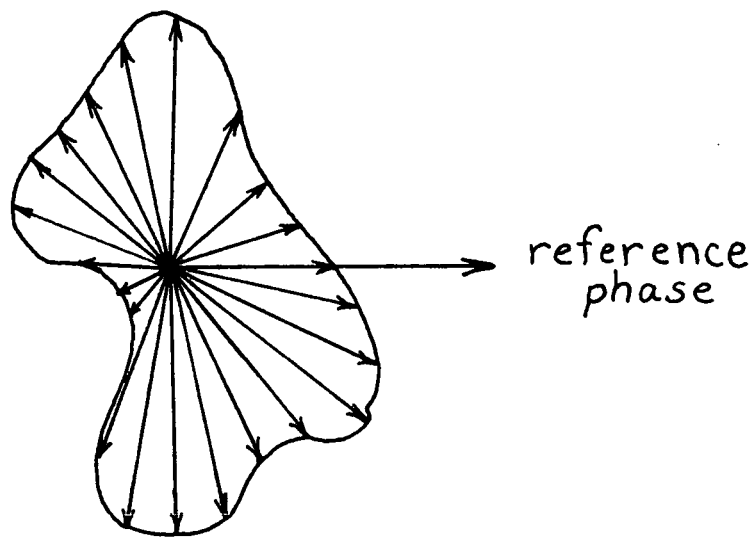

Figure B-3

Instantaneous Phase Distribution of
Incident Radiation

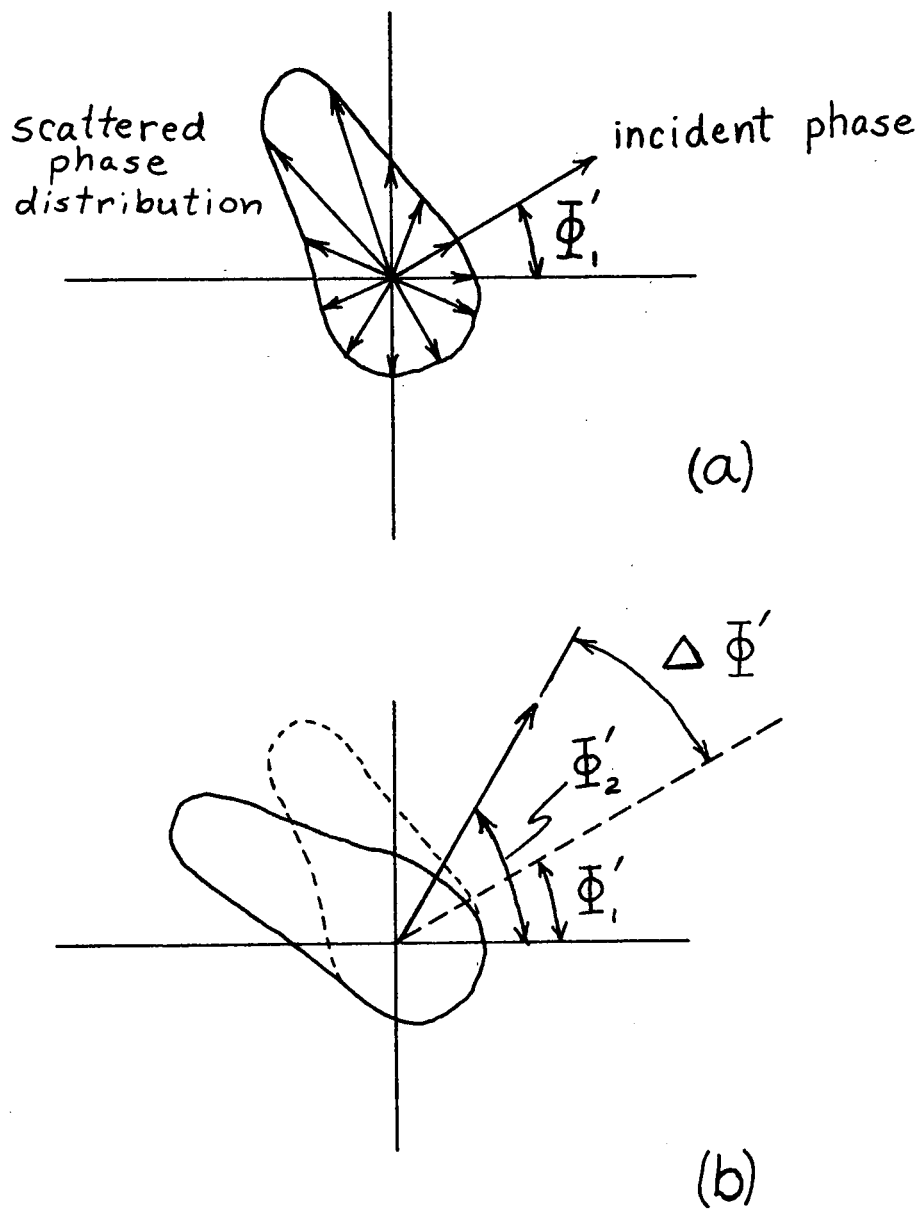

Figure B-4

Relationship of a Single Incident Phase
Component to the Scattered Phase Distribution

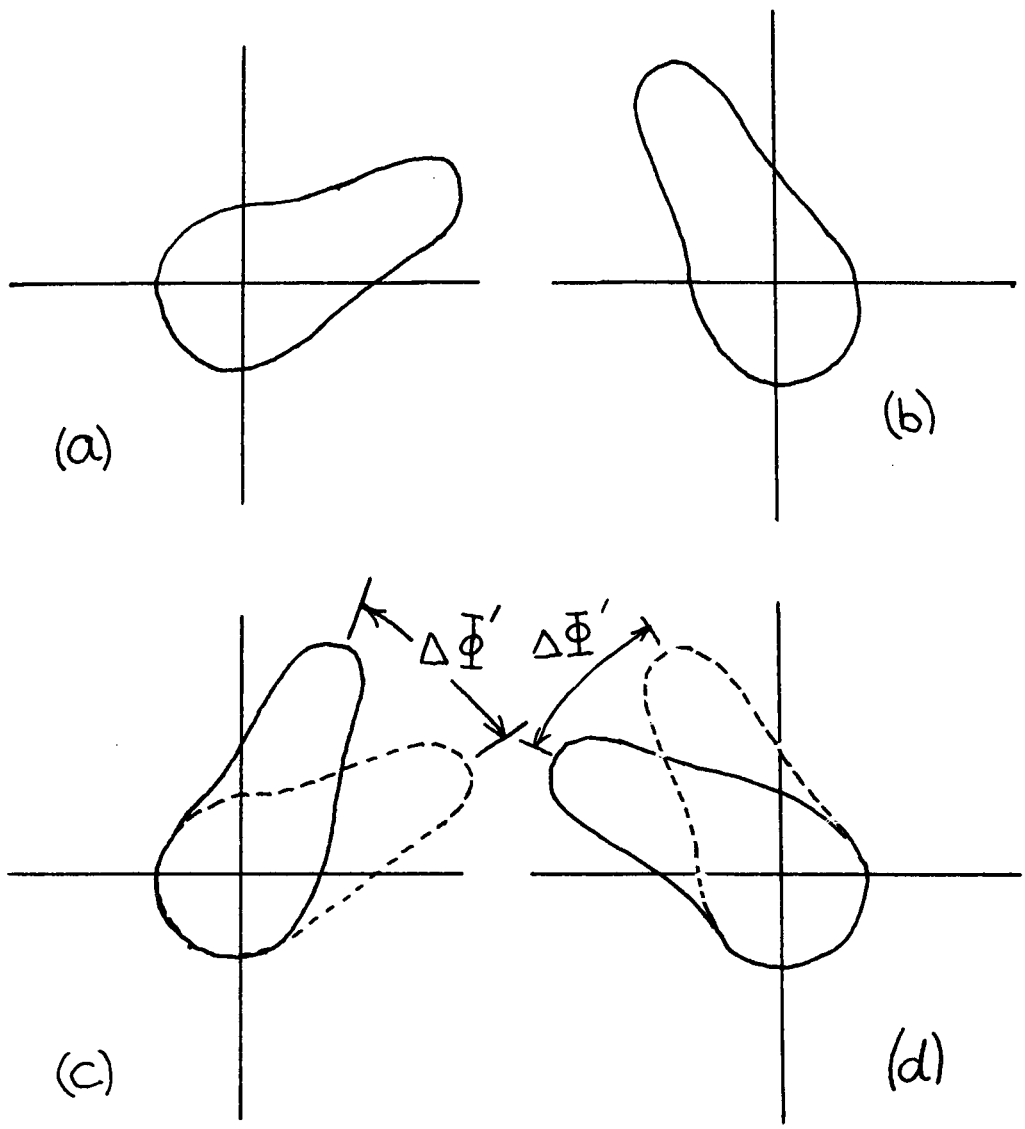

Figure B-5

Relationship of Incident Instantaneous Phase Distribution to Scattered Instantaneous Phase Distribution

incident phase distribution (Figure B-5c) produces a phase rotation $\Delta\Phi'$ of the scattered phase distribution (Figure B-5d). For a sufficient time length, the incident distribution of phases is uniform, a result of the combination of each instantaneous phase distribution. The resultant of the instantaneous scattered phase distribution is consequently uniform, since for a sufficient time span, the probability of any particular phase is the same as the probability of any other phase. Thus there is no time average phase interaction of scattered fields due to different path lengths of radiation if the incident radiation is randomly phased.